Paleoceanography and Paleoclimatology

RESEARCH ARTICLE
10.1029/2026PA005444

Laurasian Seaway History During the Early Jurassic From Quantitative Mineralogy and Detrital Zircon Dating

M. Jiang[1,2], S. P. Hesselbo[1], G. Pieńkowski[3,†], E. Krzemińska[3], J. B. Riding[4], A. Uchman[5], D. Salata[5], and C. V. Ullmann[1,6]

[1]Camborne School of Mines, Department of Earth and Environmental Sciences, University of Exeter, Cornwall, UK, [2]Office of International Cooperation and Exchange, Chengdu University, Chengdu, China, [3]Polish Geological Institute–National Research Institute, Warszawa, Poland, [4]British Geological Survey, Nottingham, UK, [5]Faculty of Geography and Geology, Jagiellonian University, Kraków, Poland, [6]State Key Laboratory of Geomicrobiology and Environmental Changes, China University of Geosciences (Wuhan), Wuhan, China

†Deceased 2023.

Key Points:

- Changes in detrital mineral characteristics are observed from an exceptional deep-water record of the Early Jurassic in the Laurasian Seaway
- Sediment provenance in the meridional Laurasian Seaway is linked to a general reversal of bottom current directions
- The largest change in sediment sources is coeval with opening of the Hispanic Corridor during the Sinemurian–Pliensbachian transition

Supporting Information:

Supporting Information may be found in the online version of this article.

Correspondence to:

S. P. Hesselbo,
s.p.hesselbo@exeter.ac.uk

Citation:

Jiang, M., Hesselbo, S. P., Pieńkowski, G., Krzemińska, E., Riding, J. B., Uchman, A., et al. (2026). Laurasian seaway history during the Early Jurassic from quantitative mineralogy and detrital zircon dating. *Paleoceanography and Paleoclimatology*, *41*, e2026PA005444. https://doi.org/10.1029/2026PA005444

Received 2 FEB 2026
Accepted 1 MAY 2026

Author Contributions:

Conceptualization: M. Jiang, S. P. Hesselbo, G. Pieńkowski, C. V. Ullmann
Data curation: S. P. Hesselbo, C. V. Ullmann
Funding acquisition: M. Jiang, S. P. Hesselbo, G. Pieńkowski, A. Uchman, C. V. Ullmann
Investigation: E. Krzemińska, J. B. Riding, D. Salata
Methodology: M. Jiang, S. P. Hesselbo, J. B. Riding, C. V. Ullmann
Supervision: S. P. Hesselbo
Writing – original draft: M. Jiang, S. P. Hesselbo, E. Krzemińska

Abstract

The Laurasian Seaway comprises a N-S oriented trans-Pangaean corridor linking Tethys to the Boreal Sea during the Jurassic, and direction of water flow has been the subject of considerable debate. The Llanbedr (Mochras Farm) borehole, Cardigan Bay Basin, Wales, is a uniquely informative record that comprises an expanded deep-marine silty argillaceous succession of Early Jurassic age. Deposition there is inferred to have been from contour currents under conditions that were deeper and more open than the restricted basins of the eastern seaway. Quantitative mineralogy and detrital zircon ages define five mineral assemblage units. Units 1 and 2 (Hettangian–Sinemurian) have mixed age spectra including abundant pre-Cadomian zircons (>950 Ma) sourced from the north; associated mineralogy includes high albite and biotite content indicating lack of chemical weathering. Unit 3 (uppermost Sinemurian) is similar to strata below but contains mostly Caledonian zircons (~460 Ma) of more local origin. Unit 4 (Pliensbachian) has predominance of Cadomian zircons (750–540 Ma), and quartz-rich sediment. The Unit 4 base corresponds to a sea-level rise and opening of the E-W Hispanic Corridor connecting equatorial Panthalassa with Tethys and change in configuration of sediment transport with sourcing postulated from the south and west. Unit 5 (uppermost Pliensbachian–Toarcian), shows greater dominance of Cadomian zircons coincident with severe global change at the Pliensbachian–Toarcian boundary and Toarcian Oceanic Anoxic Event. Timing and direction of inferred provenance change suggests that seaway circulation was strongly influenced by the opening of the Hispanic Corridor at the Sinemurian–Pliensbachian boundary and relatively stable thereafter.

Plain Language Summary

About 200 million years ago the continents were merged into a single supercontinent, Pangaea. As the supercontinent broke up, it was crossed by N-S and E-W oriented seaways and oceanic corridors that strongly affected ocean and shelf circulation. Here we present mineralogical data from a unique borehole location in NW Europe and document marked changes in sediment types and sources that can be linked in particular to opening of the E–W oriented Hispanic Corridor, a major event in the break-up history of the supercontinent.

1. Introduction

The Jurassic rift basins of NW Europe, Greenland and the eastern North American seaboard are amongst the most studied Jurassic successions in the world (e.g., see overviews in Morton et al., 2025; Pieńkowski et al., 2008; Surlyk et al., 2021). Following marine transgression across the region in the Early Jurassic, these basins linked up to form a N-S oriented Laurasian Seaway that provided a conduit for water exchange between the north polar region (Boreal Sea) and the equatorial oceanic realm of the Tethys (Figure 1; Bjerrum et al., 2001; Dera & Donnadieu, 2012; Pieńkowski et al., 2021, 2024; Rossi et al., 2023; van de Schootbrugge et al., 2019).

From physical oceanographic modeling, the flow through the seaway was suggested to have reversed from a southerly to northerly source during the Early Jurassic (Bjerrum et al., 2001; Dera & Donnadieu, 2012) or to have been slowed or been occluded by tectonic uplift in the North Sea region (see Archer et al., 2019; Underhill & Partington, 1993), thereby affecting marine temperature and heat transport in the seaway, and triggering major cooling of the Arctic in the late Pliensbachian and late Toarcian stages in a positive feedback loop (e.g., Korte et al., 2015). Additionally, the opening of an E-W equatorial marine connection during the Early Jurassic directly linking Panthalassa and Tethys, the Hispanic Corridor (Aberhan, 2001, 2002; Damborenea et al., 2013; Porter

Writing – review & editing:
S. P. Hesselbo, A. Uchman, C. V. Ullmann

et al., 2013), is further considered to have affected water flow within the Laurasian Seaway (Ruvalcaba Baroni et al., 2018, their Figure 4), but in an opposite direction to that suggested by Bjerrum et al. (2001).

Evidence from the sedimentary record supporting or contradicting these predictions of large-scale change in bottom currents through the seaway has been hard to come by. Our study site, the Llanbedr (Mochras Farm) borehole in North Wales, Cardigan Bay Basin (Figure 1; Copestake & Johnson, 2014; Dobson & Whittington, 1987; Hesselbo et al., 2013; Wood & Woodland, 1968; Woodland, 1971) is uniquely useful in this regard. Recently, it has been recognized that the mudstone/siltstone sedimentary facies recovered from Mochras are much less restricted paleoceanographically than other basins lying to the east of the seaway (e.g., Percival et al., 2016; Os-isotopes), and that deposition was in a deep-water (below storm wave base) contourite setting that has the potential to indicate long-distance sediment transport directions and variations in flow strengths through the Early Jurassic (Pieńkowski et al., 2021, 2024; sedimentary facies and ichnology). Although the Mochras borehole has provided geochemical data that have been used to document paleoenvironmental change and infer astronomical timescales (e.g., Fendley et al., 2024; Hudson et al., 2025; Pieńkowski et al., 2021, 2024; Ruhl et al., 2016, 2022; Storm et al., 2020; Ullmann et al., 2022; Xu et al., 2018), except for clay minerals (Deconinck et al., 2019; Munier et al., 2021) mineralogical characterization of the core has largely been lacking up to this point.

Jurassic sediment in the UK region is preserved in major extensional fault-controlled basins, where the marine Early Jurassic Lias Group generally rests on marginal marine strata of the Late Triassic Penarth Group (e.g., Ambrose, 2001; Cope, 1995; Cope et al., 1980; Hesselbo, 2012; Warrington et al., 1980). Basin initiation is generally of Permian age and the pre-Jurassic fill comprises continental detrital or evaporitic facies (Newell, 2018; Tappin et al., 1994; Ziegler, 1990). In the Late Triassic, marine influence on sedimentation became dominant, with a fully marine environment established just before or at the start of the Jurassic period (Cope, 1984; Hesselbo et al., 2004; Mayall, 1981). In the UK area Jurassic marine sedimentation is characterized by offshore marine deposition modulated by episodic regional and supra-regional progradation of shallow water facies at times of relative sea-level fall (Hallam, 1969, 1981, 2001; Hesselbo, 2008; Hesselbo & Jenkyns, 1998; Tappin et al., 1994).

The Cardigan Bay Basin, located adjacent to the north-western part of the Welsh Massif, is constrained by a series of normal faults at its eastern and south-eastern edges, including the Mochras, Tonfanau, and Bala faults (Figure 1; Dobson & Whittington, 1987; Tappin et al., 1994; Woodland, 1971). These faults are thought to have had a Paleozoic origin and may have then been re-activated more than once (Chadwick & Evans, 2005; Tappin et al., 1994). The Mochras Fault is hypothesized to be an important structure controlling thick sedimentary successions in the Cardigan Bay Basin through the Permian, Triassic, Jurassic, and into the unconformably overlying Cenozoic (Tappin et al., 1994; Wood & Woodland, 1968), although there is no direct evidence of synsedimentary fault activity in the Jurassic record at Mochras. Sedimentation rates in the order of ∼4–7 cm/kyr have been estimated for Mochras (Hudson et al., 2025; Pieńkowski et al., 2021, 2024; Ruhl et al., 2016; Storm et al., 2020).

Here, we present a new record of sedimentary mineralogy for the Early Jurassic argillaceous deposits at Mochras, focusing particularly on the middle Sinemurian to upper Toarcian part of the Mochras core where intact core slabs are best preserved. We present two complementary mineralogical data sets that can be used to infer sediment provenance and paleoclimatic conditions in the sediment source areas: (a) a quantitative mineralogical data set based on elemental maps converted into mineral grains (using QEMSCAN) and (b) detrital zircon U-Pb ages. We note also that neither of these techniques have been commonly applied to mudstone successions, but we hope here to demonstrate their considerable potential. Using these data, we assess the mineralogical signatures of sediment provenance and paleoclimate change through this important reference core and suggest new scenarios for regional sediment transport and bottom water currents.

2. Materials and Methods

2.1. Polished Blocks and Thin Sections

The higher Jurassic (Toarcian–Pliensbachian) sections of the Mochras core (∼602–1,280 m below surface [mbs]), are mostly intact and have been sawn lengthways into half or one-third slabs which are retained in the National Core Repository of the British Geological Survey (BGS) in Keyworth, Nottingham. The complementary working

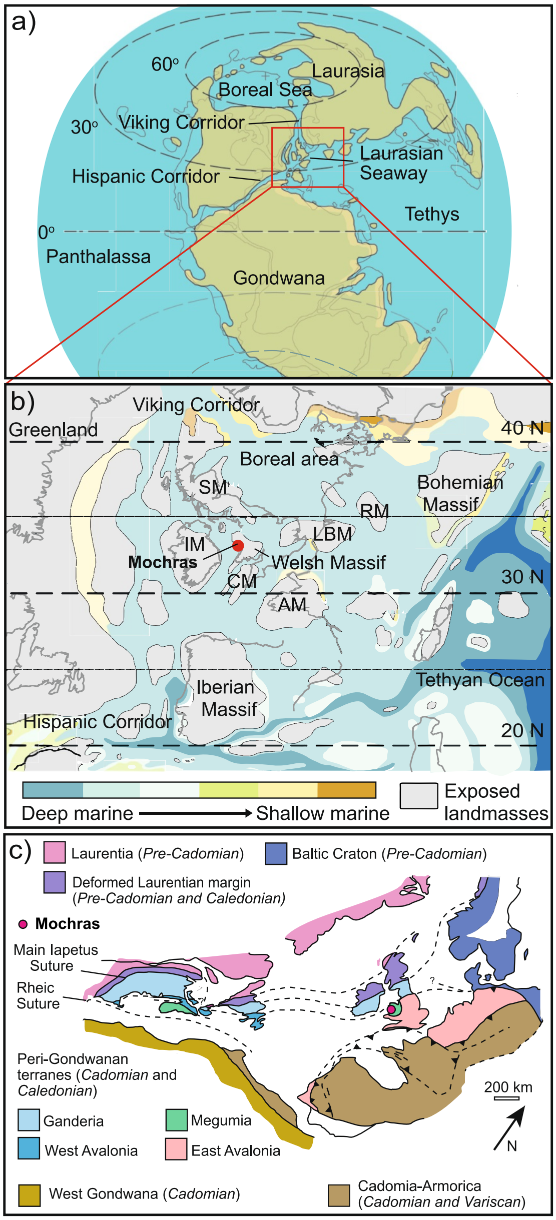

Figure 1. Paleogeography and location maps. (a) Early Jurassic global paleogeography, based on Dera et al. (2011); (b) Paleogeographic details of the NW Tethyan region showing the Mochras locality (red spot) at the NW margin of the Welsh Massif in the southern central area of the Laurasian Seaway (map modified from Dercourt et al., 2000), reused with permission from the Commission for the Geological Map of the World; (c) Principal potential sediment source terranes in the British Isles region as configured prior to North Atlantic seafloor spreading (based on Landing et al., 2022); sources of pre-Cadomian zircons lie principally to the north of the Mochras depositional site (Laurentia/Baltica) whilst sources of Cadomian zircons lie to the south (Peri-Gondwanan terranes and Cadomia-Amorica). Sources yielding Caledonian zircons are principally the deformed Laurentian margin, Ganderia, and Megumia. It is important to note that considerable local heterogeneity exisits within these terranes, for example, significant Cambrian-Ordovician magmatism (~450–520 Ma) occurred on the Gondwanan margin with ages that overlap with Caledonian events (Casas & Murphy, 2018).

parts for this upper interval, and nearly the entire core further below (Sinemurian–Rhaetian, ∼1,280–1,930 mbs), were broken up soon after recovery. These cm-scale core fragments were aggregated into 5-foot (∼1.4 m) intervals (“reserve” bag samples) and provide the opportunity for further analyses, albeit with reduced stratigraphic precision.

The core also yielded several thousand rock specimens that were considered of special (largely paleontological) value, and which were registered into the BGS collections with precise depths recorded (“registered specimens”). All these materials are also archived at the National Core Repository. Thin sections and rock blocks were prepared from all these materials for the present study with the highest resolution in the Pliensbachian Stage, currently the most data-rich interval of the borehole.

Working up-section, for quantitative mineralogy, 12 samples were prepared from Hettangian strata (1,905–1,742 mbs), 38 from the Sinemurian (1,742–1,260 mbs), 83 from the Pliensbachian (1,260–865 mbs), and 25 from the Toarcian (865–700 mbs). The highest stratigraphic resolution, in the Pliensbachian, is 1–2 m from ∼1,068 to 865 mbs and 1–4 m from ∼1,260 to 1,068 mbs, with a median of 2.4 m.

For the preparation of polished blocks, selected rock materials were dry cut to fit in a 30 mm-diameter plastic mold which was then filled with Struers Epofix two-part cold mounting resin. The samples were kept at room temperature for at least 24 hr for the resin to consolidate. To avoid uneven pressure on the sample which potentially influences the polishing surface quality when automatically grinding by machine, the back side of the sample blocks was manually ground first until a flat surface was achieved. The samples were processed on a Kemet Forcimat sample holder attached to a Forcipol 300 1V grinder and polisher using a pneumatic force of ~ 1–4 N with pressures modified according to polishing step and lithology. The grinding was carried out using silicon carbide polishing paper with 240, 400, 800, 1,200, 2,500, and 4,000 grit. Each stage was accompanied by a gentle wipe of the sample surface by tissue to eliminate impurities and loose grains. Additional thin sections were mechanically polished using minimal water during grinding and polishing to prevent the loss of clay. All samples were carbon coated with a 25 nm-thick carbon layer for later Scanning Electron Microscope (SEM) observation. Example SEM images are shown in the Supporting Information S1 file.

2.2. Quantitative Mineralogy

Integrated petrological observation of samples was carried out using automated mineralogy (QEMSCAN®) technology. QEMSCAN® (Quantitative Evaluation of Minerals by Scanning Electron Microscopy) allows mapping of grains from elemental compositions, including attributes such as texture, shape, size and constituent mineral phases. The system used in this study is integrated with an FEI Quanta FEG SEM 650 SEM and uses a combination of back-scattered electrons and energy dispersive X-rays. The spatially resolved X-ray spectra within a targeted region on the sample surface are interpreted as mineral composition by the software package “iDiscover.”

For this study, the “field scan” mode was chosen for comprehensive mineralogical observation. Spectra were collected with 1,000 total X-ray counts per pixel at 0.5 μm spacing for each sample and compared to an in-house Species Identification Protocol that discriminates minerals based on their characteristic X-ray and electron backscatter intensities. Total areas measured were ∼6 mm^2 per sample, which equates typically to a notional ∼6,000 grains in a fine siltstone, and an analysis time of ∼14–17 hr. Analyses were carried out using a 10 nA electron beam current accelerated to 15 kV and focused to 4.8–5.6-unit beam diameter depending on current output. Prior to each analysis, standard instrument tuning was performed, including beam focusing, beam alignment and calibration of the X-ray and backscatter detectors.

All quantitative mineralogy data are available from the UK National Geoscience Data Center (Jiang et al., 2026a).

2.3. Grain Size Analysis Using ImageJ

Based on the 6 mm^2 SEM image generated during QEMSCAN scanning, the Java-based image processing program ImageJ was used for the calculation of the proportion of minerals in various gray scales (Schneider et al., 2012). "Median grain size" was chosen to describe the size distribution of the quartz population. This normally corresponds to the grain that is encountered at the 50% weight mark when sorting the grains in the sample from the smallest to the largest (Folk & Ward, 1957). The calculation was modified by using area instead of weight in this study. As the most abundant detrital mineral, typically ∼1,300 quartz grains were observed in the quantified fraction of each sample. Due to this comparatively large number of grains, the median grain size of quartz is considered to give a robust estimate of average grain size evolution. The median measure is taken to be superior to average or maximum grainsize as it is not as liable to minor misidentification of small quartz grains, or the random encounter of large detrital grains in the limited area studied. The diameter of individual grains was calculated as the square root of their area and is therefore not an entirely accurate representation of their true diameter but provides a reproducible, and comparable measurement. All grain size data generated by this method are available from the UK National Geoscience Data Center (Jiang et al., 2026a).

2.4. Detrital Zircon Sampling and Preparation

Each sample was taken from the "reserve" bags to allow for sufficient mass to be processed. Two batches of samples were collected: those numbered herein 1–50 were taken principally from the Pliensbachian, but range across almost the whole Lower Jurassic profile. Those samples numbered 101–110 are from between 900 and 600 mbs (mostly Toarcian). Lithologically, the samples represent well indurated mudstone with varied carbonate content. The rock samples were crushed in a jaw crusher and the material with the fraction smaller than 1 mm was sieved. The sieved material was treated with 10% HCl in a water bath to remove carbonate, and after that 30% hydrogen peroxide was used to remove organic matter. No chemical dissolution of the excess pyrite was applied. The residue remaining after chemical treatment was washed on a sieve with a mesh of 30 μm. Sediment within the fraction greater than 30 μm was sieved and the 30–125 μm fraction was used for further analyses. Two samples (47 and 48, Toarcian) are notable because after chemical dissolution the obtained material was sticky and increased in volume, which suggests that the rocks contain a higher content of swelling clay minerals of the smectite type.

For optical observation the heavy fraction was separated in heavy liquids (sodium polytungstate with a density of 2.90 g/cm^3) from each 30–125 μm sample. Zircon grains were collected from the separated heavy fraction by handpicking using a binocular microscope. All potentially useful grains were selected from the concentrate, even damaged (or uncertain) zircons. More than 1,700 zircons in total were extracted from the Mochras samples.

Zircon grains for age analyses were collected only from samples meeting a minimum quantity criterion of 30 grains. All zircon grains from the samples meeting that requirement were transferred directly from the container to an adhesive tape. The zircon crystals were then mounted in epoxy resin together with Temora 2 standard grains with $^{206}Pb/^{238}U$ age of 416.8 ± 0.3 Ma (Black et al., 2003), accompanied with reference 91,500 zircons used for elemental concentrations U = 82.5 μg/g (Wiedenbeck et al., 2004). The megamounts (disc of 3.5 cm diameter) usually contained 4 to 5 samples accompanied with the Temora 2 and 91,500 reference zircon grains. After the resin had hardened, the mounts were polished until quasi-central grain sections were obtained.

The grains from each sample were documented in reflected light and transmitted light on a Nikon ECLIPSE LV100POL optic microscope accompanied with NIS-Elements software. Polished surfaces were cleaned with ethanol and Milli-Q deionized water. Zircon mounts were then prepared for SEM cathodoluminescence (SEM-CL) imaging using the Hitachi Su 3,500 with CL detector. Zircon mounts were coated with a 2 nm thick layer of high purity gold using a Quorum Q150 T PLUS vacuum coater. Before isotopic measurement, the gold film was removed and the mount re-cleaned and dried overnight in an oven at 30°C, prior to being recoated with about 15 nm of high purity gold (i.e., 99.999%) for sensitive high resolution ion microprobe (SHRIMP) analysis using a Quorum Q150 T PLUS vacuum coater.

2.5. Dating of Zircons

The U-Pb zircon age analyses were conducted on the SHRIMP IIe/MC instrument at the Polish Geological Institute, Warsaw, using a duoplasmatron as primary ion source, according to the general procedure described by Williams (1998). The measurements were performed during two independent cycle-sessions, but according to the same procedure and settings. Secondary ions were collected on a single electron multiplier by cycling the magnet through six scans on nine masses: $^{196}Zr_2O$, ^{204}Pb, 204.1 (as a background), ^{206}Pb, ^{207}Pb, ^{208}Pb, ^{238}U, ^{248}ThO, and ^{254}UO.

Prior to each measurement, the surface of the analysis site was pre-cleaned by rastering of the primary beam for 2 min, to eliminate surface common Pb (Pbc). The acquisition time for each spot was 15 min, forming an elliptical crater with spot size 20 × 23 and 4 μm depth. During each analytical session data were collected across the mount in a sequence consisting of one analysis of a Temora-2 reference zircon measurement after every fourth unknown sample analysis. The ^{238}U-^{206}Pb reference material of Temora 2 (416.8 ± 0.3 Ma), analyzed usually from 14 to 21 spots during each session, yielded $^{238}U/^{206}Pb$ reproducibility (1σ) in range of 0.75%–0.80%, indicating good stability. The $^{238}U/^{206}Pb$ calibration uncertainty (1σ) is given within Data File 2. These values covered the range from 0.20% to 0.95%.

The raw data reduction and error assessment were carried out using the Squid 2.5 software (Ludwig, 2009). The U-Pb zircon age data are available from the UK National Geoscience Data Center (Jiang et al., 2026b). Errors given on single spot analyses are based on counting statistics, are at the 1σ level and include the uncertainty of the standard added in quadrature. To construct the concordia curves and probability plots showing an age distribution, Isoplot 3.71 (Ludwig, 2012) was used. All plots are shown in the Supporting Information S1 files.

Pbc corrections for unknown samples were based on measured ^{204}Pb. The isotopic composition was calculated using the Pb isotopic evolution model of Stacey and Kramers (1975), and the age corresponding to the preliminary $^{206}Pb/^{238}U$ age was calculated using the default Pbc compositions. Individual analyses with >5% (Pbc), were not considered for interpretation. The concordia distance (d_c), that takes into account the uncertainties of the U-Pb isotopic composition (Vermeesch, 2021) has been used as a discordance filter. To obtain an age spectrum for each sample the $^{206}Pb/^{238}U$ ages for zircon grains <1,000 Ma, and $^{207}Pb/^{206}Pb$ for those >1,000 Ma were used. This is a consequence of the relatively short half-life of the ^{235}U parent, making $^{207}Pb/^{206}Pb$ ages less precise than $^{206}Pb/^{238}U$ ages for relatively young zircons (Black et al., 2003; Gehrels, 2012). Moreover, the ages of the potential source rocks are most often presented in publications using this assumption.

3. Results

3.1. Major Mineral Trends

Based on the stratigraphic distributions of the major and minor minerals described below, combined with the results from the detrital zircon ages described in Section 3.2, five major mineral assemblage zones are recognized (summary in Table 1).

Due to a relative sparsity of data through the lowest part of the core, we do not describe Unit 1 in detail, but recognize it based on major changes in carbonate content, predominantly calcite, already described elsewhere (Figure 2; Ullmann et al., 2022). Across other basins in the UK this compositional change corresponds to a widespread lithostratigraphic transition from an underlying limestone-rich formation, the Blue Lias, to an overlying relatively limestone-poor formation, the Charmouth Mudstone (Cox et al., 1999).

Long-term shifts in carbonate content exert the strongest control on the large-scale trends in mineral quantity at Mochras, as evidenced here and in previous studies using X-ray fluorescence and X-ray diffraction methods (Deconinck et al., 2019; Ruhl et al., 2016; Storm et al., 2020; Ullmann et al., 2022). Beginning in the Turneri Zone (mid Sinemurian; ∼1,500 mbs), carbonate content is comparatively low, averaging ∼25% (Figure 3). Carbonate content shows distinct fluctuations up-section but remains low into the Oxynotum Zone in the upper Sinemurian, with lowest values encountered in the upper Obtusum Zone (∼1,380 mbs).

Table 1
Key Attributes of Mineral Assemblage Units in the Lower Jurassic of Mochras Based on Major and Minor Mineral Abundances Together With Detrital Zircon Ages

Mineral Assemblage units	Depths meters below surface (mbs)	Carbonate (low = <35%; high = >35%)	Detrital minerals	Zircon samples	Zircon ages	Stages
5	870–605	Low	Low K-feldspar, low biotite, high muscovite in lower part, moderate albite, moderate quartz	46–50, 102–110	750–540 Ma dominance (Cadomian)	uppermost Pliensbachian—Toarcian
4	1,260–870	High	High K-feldspar in higher part, low biotite, moderate to high muscovite, moderate to high quartz	29–45, 101	Mixed but with high 750–540 Ma (Cadomian)	Pliensbachian
3	1,340–1,260	High	High K-feldspar, moderate albite, low muscovite, low biotite	25–28	Mixed. Local 490–390 Ma dominance (Caledonian)	uppermost Sinemurian
2	1,620–1,340	Low	High biotite, high albite	10–24	Ave. >950 Ma (Pre-Cadomian)	middle–upper Sinemurian
1	1,910–1,620	High	Not determined	1–9	Ave. >950 Ma (Pre-Cadomian)	Hettangian—lower Sinemurian

Carbonate content rises to about 40% for the latest Sinemurian section at the base of Assemblage Unit 3, and shows wide variation through the Pliensbachian, likely due to Milankovitch-forced paleoclimate change (e.g., Hollaar et al., 2021, 2023; Ruhl et al., 2016). Pliensbachian strata are also characterized by two long-term shifts in carbonate content, with optima averaging ∼60% in the Jamesoni and Margaritatus zones, and lowest values of ∼25% in the middle Pliensbachian (at the Ibex–Davoei zonal boundary). Carbonate content for the uppermost Pliensbachian (Spinatum Zone) shows an abrupt decline, corresponding to the base of Mineral Assemblage Unit 5, reaching lowest values ∼5% in the lower Serpentinum Zone of the lower Toarcian. Carbonate content gradually recovers to about 40% in the mid Toarcian strata.

Quartz grain size exhibits clear long-term trends. The median quartz grain size as determined by image analysis of polished blocks ranges from medium to coarse silt (Figure 3). The Sinemurian Units 2 and 3 show relatively variable grain size, but we lack sufficient data resolution to identify bed-scale variations systematically. The Pliensbachian strata of Unit 4 show a marked progressive coarsening up from medium silt at the base to coarse silt at the top, in agreement with visual core descriptions (Pieńkowski et al., 2021). A flattening of the coarsening trend in the middle Pliensbachian correlates to reduced carbonate content and increased muscovite and albite (Figure 2). Unit 5, uppermost Pliensbachian (Spinatum Zone) and Toarcian, is again finer (medium silt), but shows considerable spikey variability.

Quartz content within the largely detrital non-carbonate fraction shows similar patterns, with first-order peaks and troughs of abundances in carbonate and quartz closely coincident, an observation interpreted by Hollaar et al. (2023) as a result of the integrated effects of both strengthened and weakened seasonality during maximum precessional climate forcing in the seaway hinterland. Increase in quartz content is more gradual than carbonate across the base of Unit 3, but the decline in quartz across the base of Unit 5 is very similar to that seen in carbonate content (Figure 3).

Peaks in K-feldspar content mostly co-occur with peaks in quartz content, but significant enrichments to >1% in the silicate and metal oxide (rutile) mineral fractions are more restricted stratigraphically. Albite, muscovite, rutile and total clay contents generally show stratigraphic trends opposite to those of calcite, quartz, and K-feldspar (Figure 3). Higher biotite and albite content is evident for Unit 2 compared to the units above, likely reflecting mineralogically less mature assemblages (i.e., less strongly weathered).

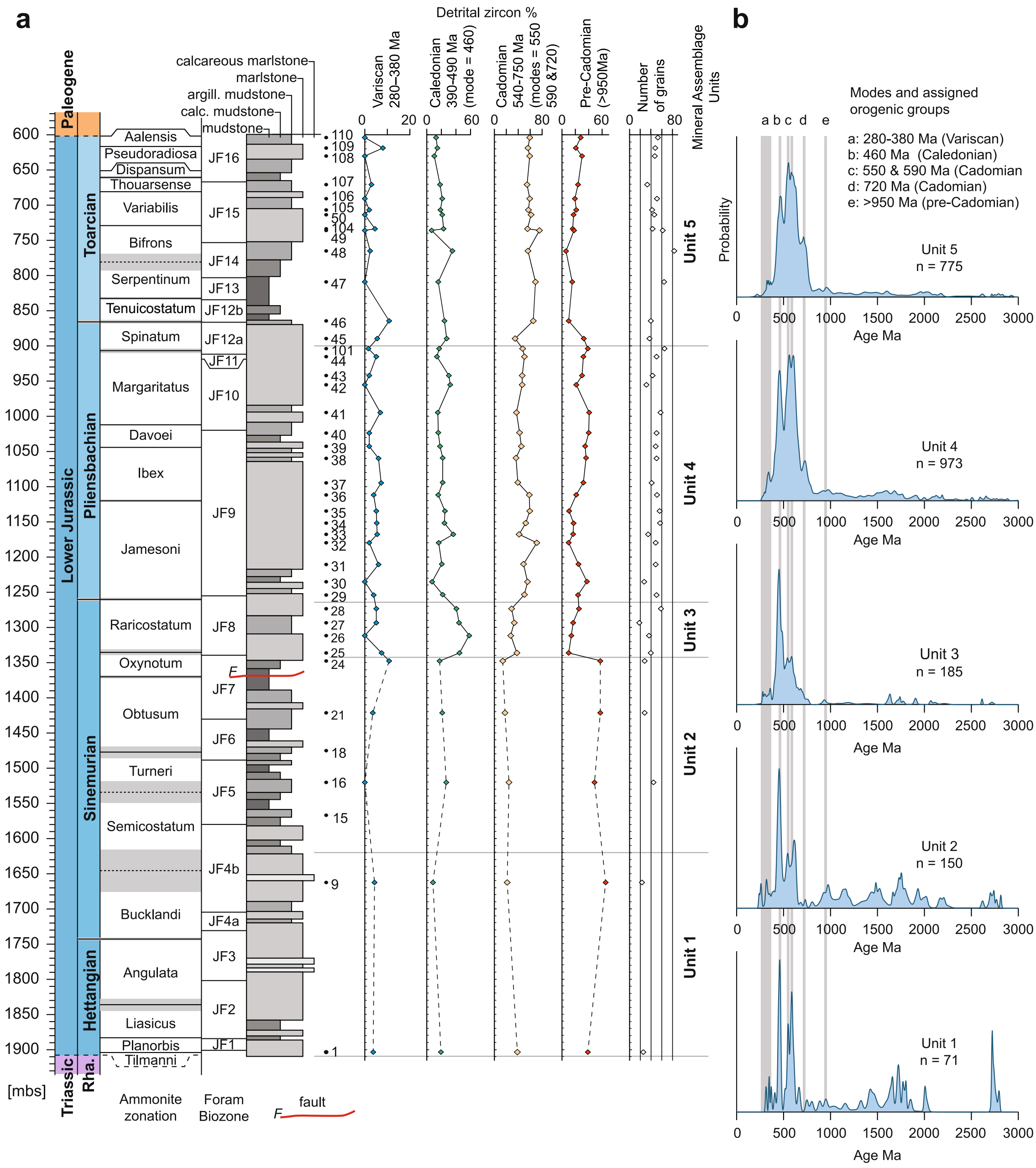

Figure 2. Summary ammonite biochronology (Copestake & Johnson, 2014; Hesselbo et al., 2023; Pieńkowski et al., 2024) lithology (Ullmann et al., 2022), and sample levels for this study, together with detrital zircon age populations grouped according to orogenic affinities. Age spectra are compiled for each mineral assemblage zone, the ranges defined according to Moyen et al. (2025) (Variscan), McKerrow et al. (2000) (Caledonian), and Linnemann, Pereira et al. (2008), Linnemann, D'Lemos et al. (2008) (Cadomian). Mineral assemblage zones are herein defined by abrupt and substantial changes in sedimentary mineral compositions and detrital zircon ages. The succession is complete at the ammonite zonal level, although the fault at 1,372 m is thought to cut out about 15 m of strata belonging to the lower Oxynotum Zone (Hudson et al., 2025). Uncertainties in zonal boundaries due to lack of marker taxa are indicated by gray shading.

3.2. Detrital Zircon Stratigraphic Distributions and Ultimate Origins

Zircons at Mochras have been assigned to four groups based on modal peaks for ages of formation which are linked to known major tectono-magmatic events (see e.g., Chew & Strachan, 2014; Linnemann et al., 2007, Linnemann, Pereira et al., 2008, Linnemann, D'Lemos et al., 2008, 2014, McKerrow et al., 2000, Moyen et al., 2025). These are >950 Ma (pre Cadomian), 750–540 Ma (Cadomian), 490–390 Ma (Caledonian), and 380–280 Ma (Variscan). Results are shown as a percentage of those groups, alongside age spectra for samples for

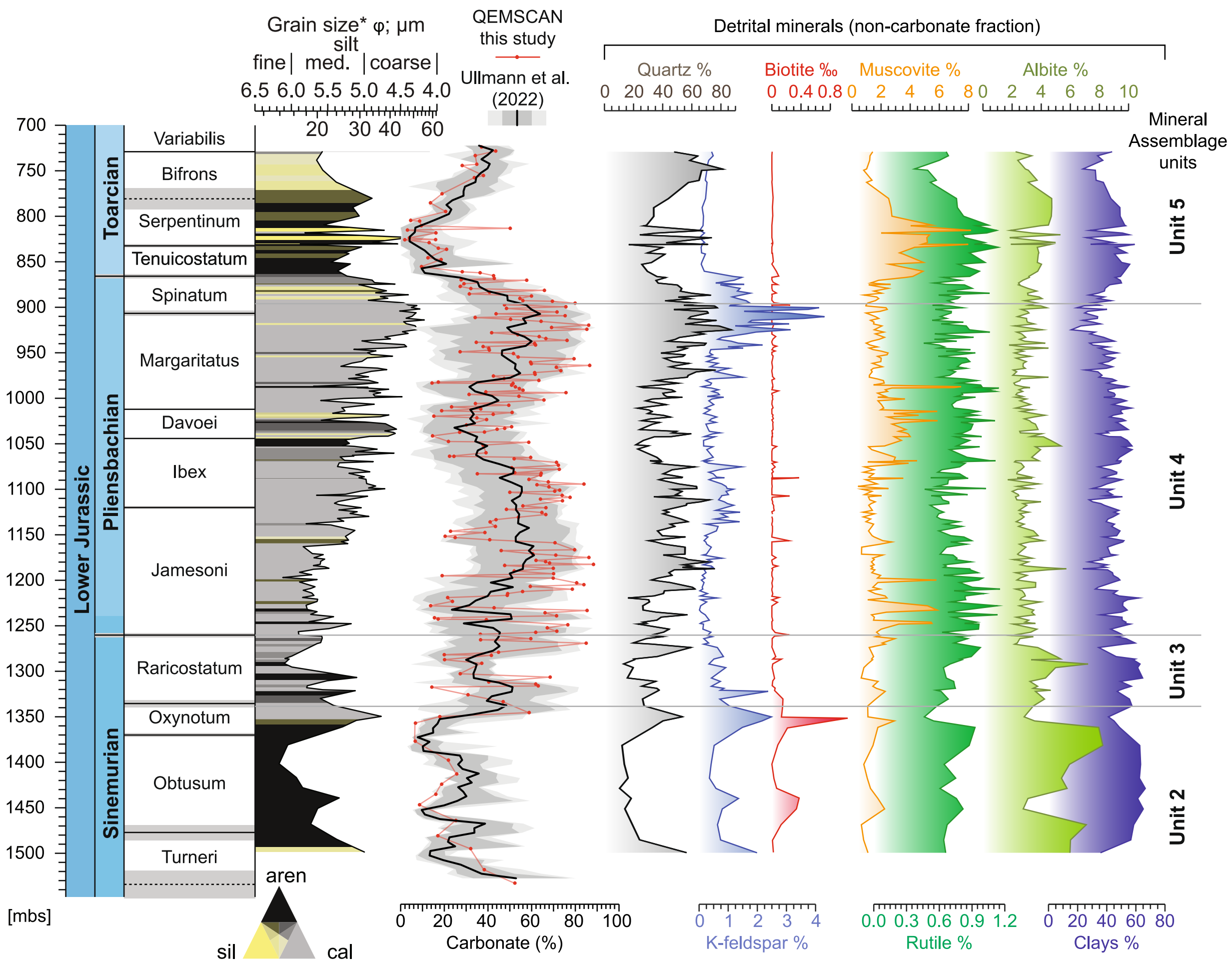

Figure 3. Overview of grain size, carbonate percentage and detrital mineral proportion from the carbonate-free fraction in mid Sinemurian to mid Toarcian part of the Mochras core determined using QEMSCAN (this study). Grain size* refers to median grain size calculation (see Section 2.3.). Mineral assemblage units are the same as for Figure 2 and are based on abrupt and substantial changes in sedimentary mineral compositions and detrital zircon ages. Detrital mineral abundances are calculated after subtraction of the carbonate fraction. Mineral polymorphs such as rutile and anatase cannot be distinguished from each other using the QEMSCAN method—here TiO_2 minerals are assumed to be rutile. aren = arenaceous mudstone, sil = siliceous mudstone, cal = calcareous mudstone.

each defined Mineral Assemblage Unit (Figure 2), and for all samples combined (Figure 4). Spectra for individual samples are shown in Data File 2. It is important to emphasize that although the assignment of age modes to specific tectono-magmatic events is an interpretation, the existence of these modes is a robust observation from our analytical results. We discuss the potential sources of zircons in more depth in Section 4.

The age data ($^{206}Pb/^{238}U$ for zircon grains <1,000 Ma, and $^{207}Pb/^{206}Pb$ for those >1,000) indicate several changes through the stratigraphic profile (Figure 2). Below ~1,350 mbs, in the Hettangian to the upper Sinemurian interval, pre-Cadomian grains dominate; though we note that these samples are relatively poor in detrital zircon. The first major change occurs in the upper Oxynotum Zone (upper Sinemurian), between Unit 2 and Unit 3 and comprises an increase in the frequency of grains of Cadomian and Caledonian age, at the expense of grains of pre-Cadomian ages. A less prominent change is observed across the Sinemurian/Pliensbachian boundary, between Unit 3 and Unit 4, where an increase in the number of Cadomian grains is noted, combined with a decrease in the frequency of grains of other age classes, especially Caledonian. The stratigraphically highest major change takes place approximately at the Pliensbachian/Toarcian boundary (~860 mbs), between Unit 4 and Unit 5, where the numbers of Variscan and Cadomian grains increase relative to pre-Cadomian grains.

Of note also are general trends (Figure 2), particularly in the Sinemurian to Pliensbachian transition (from the Oxynotum to Jamesoni biochronozones upwards) where there is a growing frequency of Cadomian grains and falling proportion (although not so consistently) of pre-Cadomian grains. Less conspicuous is a slightly growing

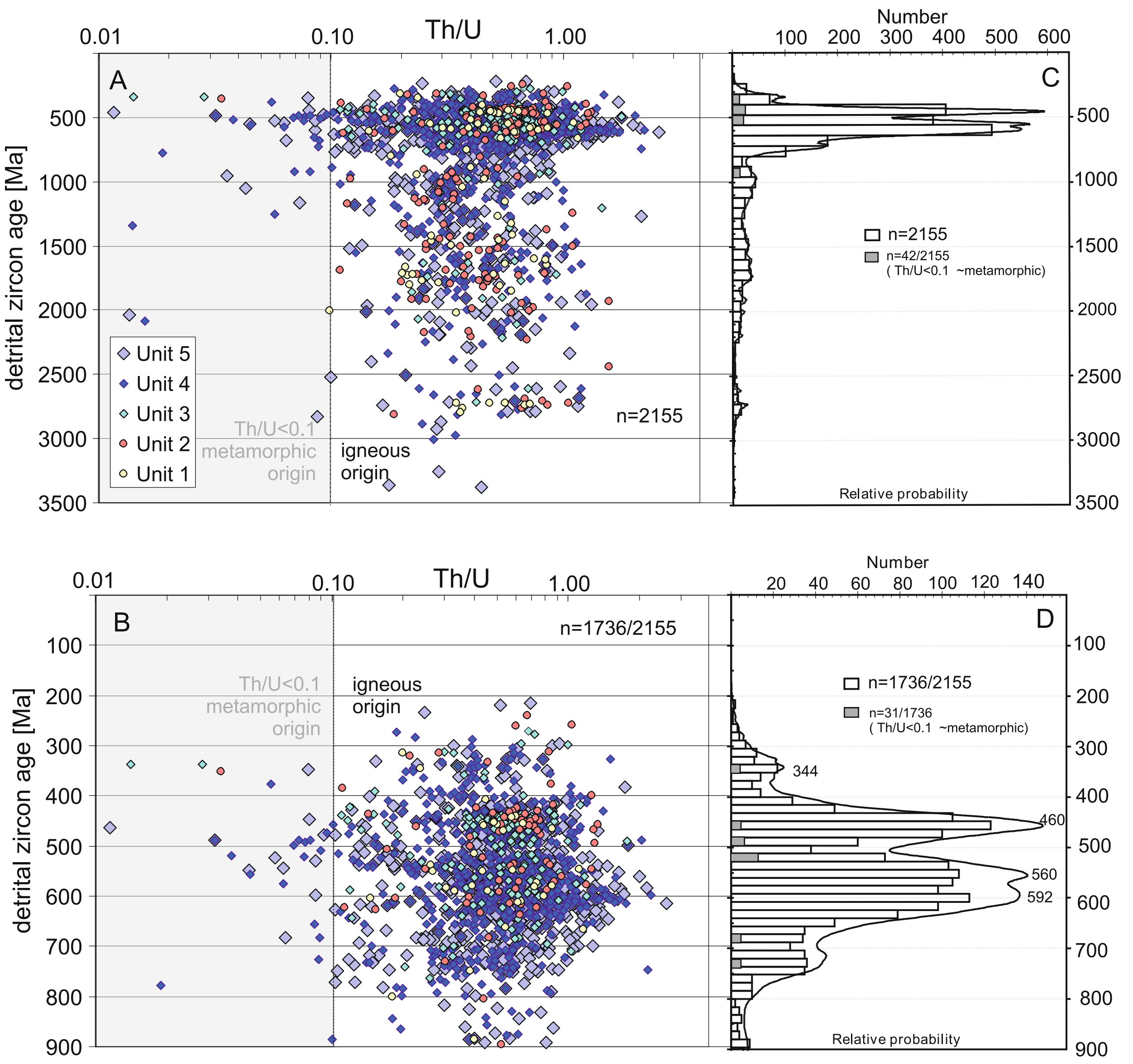

Figure 4. Compiled distribution of age data for analyzed detrital zircon samples of Mochras mudstone. Th/U versus U-Pb age diagram for (a) all detrital zircons and for (b) grains <900 Ma. Probability Density Plot of total age population for (c) all detrital zircons ($n = 2155$) and for (d) grains <900 Ma ($n = 1736/2155$). A Th/U ratio less than 0.1, which represents metamorphic zircons (e.g., Rubatto, 2017), is indicated.

trend of pre-Cadomian grains in the upper Toarcian, accompanied by a relatively high and stable frequency of Cadomian grains. Compared to other age classes, Variscan grain frequencies remain relatively low throughout the studied interval.

The pre-Cadomian age spectra from Mochras are multimodal and show considerable variations in ages of these older zircon populations, although our sample resolution for the Hettangian and most of the Sinemurian is not sufficient to resolve the stratigraphic evolution of the Precambrian components. Even though a minor proportion of zircon populations in the Pliensbachian and Toarcian, there are small increases in abundance of pre-Cadomian grains in the upper parts of each of these stages. Within the Pliensbachian and Toarcian stages three major age groups occur including an early Neoproterozoic group with the prominent double age peaks at 970 and 1,000 Ma, an early Mesoproterozoic (Calymmian) group, with the age peak at 1,500 Ma, and the Paleoproterozoic (Orosirian) group with relatively smaller number of grains peaked at ~2,000 Ma. Within the Pliensbachian the peak around 1,000 Ma is most prominent. The principal primary pre-Cadomian sources for zircons are on the margins of Laurentia, which comprises basement on the NW margins of the British Isles and further north during the Early Jurassic (Figure 1). These terrains include the metamorphic complexes of NW Scotland containing zircons with a Grenvillian (1,070–990 Ma) origin (e.g., Cawood et al., 2007; Krabbendam et al., 2017). A similar age of the source rocks also relates to the Sveconorvegian orogenic belt of southern Scandinavia (Johansson et al., 2022).

The zircon age group between 750 and 540 Ma (with a bimodal peak at 550/590, and a subsidiary older mode at 720 Ma in our data) relates to the Cadomian orogeny. Cadomian terranes formed part of the active northern margin of the Gondwana Supercontinent (Casas & Murphy, 2018; Linnemann, D'Lemos, et al., 2008, 2014). During the Early Paleozoic much of the Gondwanan margin split away as mainly Avalonian terranes that accreted on the southern margin of Laurentia. Thus, in the Jurassic these potential sediment sources lay mainly in the S of the British Isles area and to the south and west (Armorican Massif, central western Iberia and Ganderia-Megumia, East Avalonia and west Avalonia; Figure 1; Clarke et al., 2024; Fairey et al., 2018; Landing et al., 2022).

Caledonian zircons are dominant in Unit 3, but they are a distinct component of all units (Figure 2). The Caledonian orogeny occurred between 490 and 390 Ma, during the closure of the Iapetus and Tornquist oceans and the collision of the continents and terranes of Laurentia, Baltica, and Avalonia (e.g., Landing et al., 2022; McKerrow et al., 2000; Pharaoh, 2018). Zircon-bearing rocks affected or formed by the Caledonian Orogeny occupy a wide SW-NE oriented swath across the British Isles either side of the Iapetus Suture across Ireland and the England/Scotland border (e.g., Chew & Stillman, 2009; Moecher et al., 2023) and Caledonian magmatic activity was locally superimposed upon Cadomian basement. Zircons with Caledonian age signatures may ultimately have been derived from igneous rocks of this belt.

Variscan-derived zircons are sparse in all mineral assemblage units (Figure 2). The Variscan orogeny, <380 Ma, resulted from the continental collision between Laurasia and Gondwana, closing the Rheic Ocean and predominantly affecting the southern UK and much of northern and western Europe (Pharaoh, 2018).

The Th/U ratios of zircon grains can be used to classify them according to their stage of crystallization to enable differentiation of the magmatic or metamorphic provenance of zircon populations (e.g., Rubatto, 2017; Yakymchuk et al., 2018). Detrital zircon from all five units overwhelmingly originated from the felsic rocks (Th/U > 0.1) of different ages and orogenic sources (Figure 4). Metamorphic zircons (Th/U < 0.1) were evidently supplied mainly from denudation of the Cadomian host rocks (Figures 4a and 4b).

4. Discussion

4.1. Zircon Ages and Sediment Provenance—General Considerations

Zircon ($ZrSiO_4$) is a durable mineral both physically and chemically, widely used in provenance studies and commonly found in clastic sediments (Cawood, Nemchin, et al., 2003, 2004, 2007; Hawkesworth et al., 2010; Linnemann et al., 2007; Rainbird & Ernst, 2001). The age of a single zircon grain is considered the crystallization age of the rock in the source terrain and, at regional to global scales, orogenic events play a crucial role in zircon formation due to their association with the substantial production of mainly magmatic zircon-bearing rocks (Linnemann, Pereira et al., 2008, Linnemann, D'Lemos et al., 2008).

Zircon grains may be recycled many times before the last deposition (e.g., Chew et al., 2020; Moecher et al., 2023). Thus, dominance of zircons with ages that match tectonic events gives a general rather than specific indication of source area. Nonetheless, age spectra may be used to pinpoint times of significant source change to the basin (e.g., Morton et al., 2021). Detrital zircons can be an indicator of the depositional age only in an active magmatic environment. In consequence, non-volcanic epicontinental rifts, such as the Cardigan Bay Basin, usually lack a component of syn-depositional magmatic activity and detrital zircon age groups are dominated by input from older sources (e.g., see Cawood et al., 2012).

The Mochras samples are largely argillaceous, a lithology that has been only rarely used for provenance studies (Leary et al., 2020; Sláma & Pedersen, 2015; Sylvester et al., 2022). Detrital zircon U-Pb age data from mudstone has been considered as an indicator for distal sources (Sláma & Pedersen, 2015), suggesting that selective sorting may occur during long sediment transport distance (~2,000 km). Recently, however, it has been emphasized that the zircon age spectra can also be independent of grain size (Leary et al., 2020) and allow reliable identification of fine-grained source rocks rather than simply distal sources (Sylvester et al., 2022).

A sedimentary deposit will contain components from multiple crystalline sources because of numerous magmatic episodes in one region, tectonic juxtaposition of rocks of different ages, mixing by confluence of drainage from multiple catchments, and recycling of older sediment and mixing with younger primary sources (Cawood, Nemchin, et al., 2003; Chew et al., 2020; Fedo et al., 2003; Garzanti, 2016; Košler et al., 2002; Moecher & Samson, 2006). Zircon age clusters are commonly used to discriminate provenance and global crustal events despite these complexities (Condie & Aster, 2010; Dickinson, 2008; Pointon et al., 2011; Thomas, 2011), but it is important to recognize the strong potential for each of these factors to influence the observed age spectra.

Several studies have attempted to identify the zircon-age and other mineralogical characteristics of specific provenance areas around the Cardigan Bay Basin, although not for the Jurassic. A study of the Carboniferous sandstones of the Pennine Basin, lying about 200 km to the NE of the study site, documented clear changing provenance directions through time based on identification of three principal sources (Morton et al., 2021). These include a northerly source with Archean, wide ranging mid-Proterozoic and Early Paleozoic grains compatible with source areas in Laurentia and Baltica (Hallsworth et al., 2000; Lancaster et al., 2017; Morton et al., 2021); (b) a western source with zircon age characteristics broadly similar to our Cadomian group and inferred to have an Avalonian origin (i.e., from terranes ultimately derived from the northern Gondwanan margin and accreted onto Laurentia in the Early Paleozoic; e.g., Nauton-Fourteu et al., 2021) and (c) a more distant southeastern Variscan source containing large numbers of Devonian and Carboniferous zircons (<380 Ma). On the basis of this analysis source terrains were postulated to have shifted from the north to the west and finally to the southeast through the Late Carboniferous (Morton et al., 2021).

Carboniferous sandstones from NE Wales show a variety of zircon age spectra that are considered, alongside evidence from rutile crystallization temperatures, to represent three provenance groups ranging from complexly recycled Devonian sandstones, long-distance transport from the SW, and long-distance transport from the north (Waters et al., 2021). Notably, a group of sandstones show modal peaks around 610–620 Ma which may be attributed to sourcing from the Monian metamorphic complex (Strachan et al., 2007; Waters et al., 2021) which also lies adjacent to the Mochras study site; however, it is noteworthy that only samples from our Mineral Assemblage Zone 2 show a modal peak that may match this source (Figure 2).

Closer still to the Mochras depositional site, detrital zircon ages have been studied from the Cambrian-Ordovician age metasedimentary rocks of the Welsh Massif (Pothier et al., 2015). Although small in number, the reported spectra show a wide range of characteristics, interpreted to have been brought about by tectonic juxtaposition during the Caledonian Orogeny.

In the Wessex Basin, lying ~250 km south of the Mochras site, zircon age spectra have been analyzed for the Triassic age Sherwood Sandstone Group yielding distinct provenances, including southerly sourcing from Cadomian terranes, dominant directly sourced Variscan zircons, and a group with a strong component of recycling from Devonian Old Red Sandstone (Morton et al., 2016).

It should be clear from the foregoing discussion that it is not possible to quantitatively tease out individual source areas from the age spectra that we report here with any confidence. Therefore, instead we emphasize the overall consistent stratigraphic trends in zircon age spectra through the Lower Jurassic at Mochras and focus on a discussion of how these trends relate to well documented contemporaneous tectonic and paleoclimatic events that must have influenced sediment dynamics in the seaway.

4.2. Tectonic and Climatic Controls on Sedimentary Systems in the Laurasian Seaway

Several tectonic and climatic events and episodes are thought to have affected sedimentation in the studied region. Below we summarize the salient factors and discuss how these may have contributed to the observed mineralogical trends.

The potential role of the N–S oriented Laurasian Seaway as a conduit for water exchange between Boreal Sea and Tethys Ocean has been much discussed (Figure 1; Arias, 2007; Baghli et al., 2022; Bjerrum et al., 2001; Dera & Donnadieu, 2012; Pieńkowski et al., 2021, 2024; Reggiani et al., 2010; Rossi et al., 2023; van de Schootbrugge et al., 2019). A hypothetical change from south-to-north before the Toarcian and north-to-south afterward is based principally on a modeling study (Bjerrum et al., 2001). Regional shifts in ammonite assemblages (Page, 2008) and oxygen isotope values from nektobenthic bivalves, brachiopods and belemnites (Hesselbo, Korte, et al., 2020; Korte et al., 2015; Korte & Hesselbo, 2011) are compatible with flow in the seaway being slowed or blocked (see

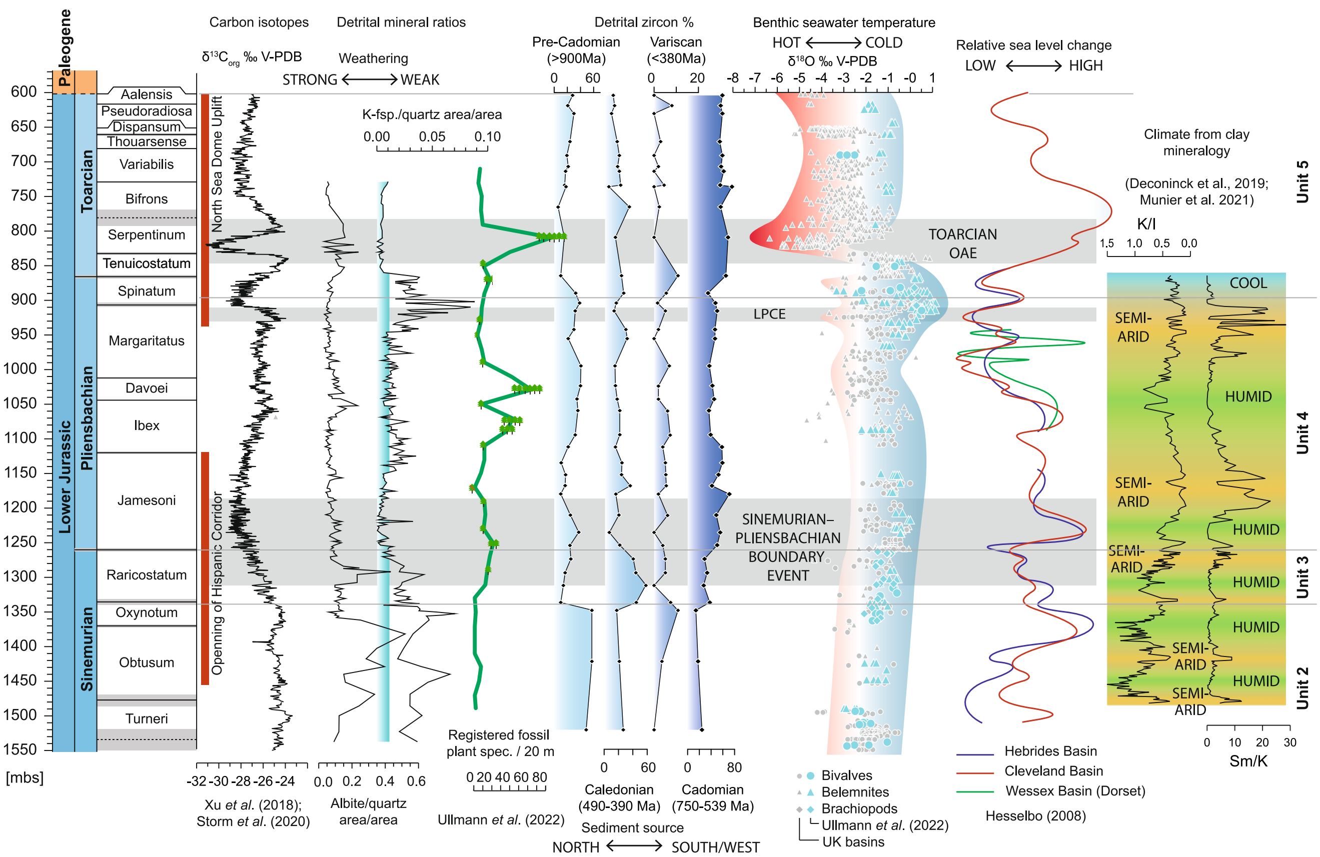

Figure 5. Summary of paleoenvironmental and provenance indicators in the Cardigan Bay Basin and wider UK region. Records shown include from left to right: Mochras carbon isotopes from bulk organic matter (Storm et al., 2020); Mochras quartz/feldspar ratios (this study); Mochras terrestrial plant macrofossil occurrences (Ullmann et al., 2022); Mochras detrital zircon provenance (this study); Mochras and wider UK region calcite macrofossil $\delta^{18}O$ as a paleotemperature proxy (Korte et al., 2015; Ullmann et al., 2022); UK basin relative sea-level change (Hesselbo, 2008), and; Mochras clay mineral ratios and inferred climate state (K—kaolinite, I—illite, Sm—smectite; Deconinck et al., 2019; Munier et al., 2021). Prominent named carbon cycle and climatic perturbations are indicated as gray bars: LPCE—Late Pliensbachian Cold Event; OAE—Oceanic Anoxic Event.

Archer et al., 2019; Underhill & Partington, 1993) in the late Pliensbachian and late Toarcian. The same effect can also be emulated by physical ocean modeling results (Dera & Donnadieu, 2012) in which it is suggested that global warming during the Early Toarcian would have slowed bottom water circulation.

As well as the meridional N–S oriented Laurasian Seaway and contiguous Viking Corridor marine strait to the north, the E–W oriented quasi-equatorial Hispanic Corridor was evidently also potentially an important factor governing water mass flow in the seaway. Physical oceanographic modeling focused on the Toarcian indicates that upon opening of the corridor, wind-driven westward flowing currents with their origins in equatorial Tethys penetrated strongly further westwards and northwards into the Laurasian Seaway (Ruvalcaba Baroni et al., 2018, their Figure 4). This strong clockwise gyre is a robust feature of all variations of the models investigated by Ruvalcaba Baroni et al. (2018). Based on paleontological evidence, opening of the Hispanic Corridor occurred substantially at the beginning of the Pliensbachian (Figure 5; Aberhan, 2001, 2002; Damborenea et al., 2013; Porter et al., 2013), although—having a tectonic origin—it is likely to have been a drawn-out event.

Inference of relative sea-level change through the Early Jurassic in and around the UK region, has been made based on sequence stratigraphy from outcrop and subsurface data (Figure 5; Copestake & Partington, 2023; Hesselbo, 2008; Hesselbo & Jenkyns, 1998; van Buchem & Knox, 1998). The major features of regional relative sea-level change are sea-level fall and coastal regression in the end-Sinemurian, late Pliensbachian and late Toarcian, alongside major sea-level rise and shoreline transgression in the early Sinemurian, early Pliensbachian and early Toarcian (Hesselbo, 2008; Hesselbo & Jenkyns, 1998). The sea-level rises, at least, have been suggested to be of global reach (Copestake & Partington, 2023; de Grasciansky et al., 1998; Hallam, 1981, 2001; Haq, 2017; Sellwood, 1972; Surlyk, 1990).

Regarding Early Jurassic climate evolution, four principal paleoclimatic events with the potential to have had a substantive effect on depositional environments in the Cardigan Bay Basin have been extensively discussed: three potential hyperthermal events and one major cooling episode (Figure 5). The earliest of these is the late Sinemurian Liasidium Event (Hesselbo, Hudson, et al., 2020; Riding et al., 2013). This possible hyperthermal event is not clearly recorded in Mochras because strata of this age are cut out by a fault at 1,372 mbs (Figure 2; Hudson et al., 2025). The following Sinemurian–Pliensbachian boundary event, characterized by a long-term negative carbon-isotope excursion (Danisch et al., 2019; Duarte et al., 2014; Ferreira et al., 2019; Jenkyns et al., 2002; Korte & Hesselbo, 2011; Schöllhorn et al., 2020; Storm et al., 2020), has been suggested to be similar to the very well documented Toarcian Oceanic Anoxic Event (T-OAE), albeit with a longer duration of about 3 Myr (Franceschi et al., 2023; Ruhl et al., 2016).

The T-OAE is a major hyperthermal event whose imprint in carbon-isotope records, reconstructed paleotemperatures, and extensive marine and lacustrine organic matter accumulation is recorded globally, marking the peak of environmental changes that began at the Pliensbachian–Toarcian boundary and extended into the mid Toarcian (e.g., Hesselbo et al., 2000, 2007; Jenkyns, 1988, 2010; Remírez & Algeo, 2020; Thibault et al., 2018). The T-OAE is considered to have been triggered by greenhouse gas release related to emplacement of the Karoo-Ferrar large igneous province (Fendley et al., 2024; McElwain et al., 2005; Ruhl et al., 2022; Svensen et al., 2007). Cooling in the late Pliensbachian has been identified but its characteristics are less well explored than for other Early Jurassic events (Bodin et al., 2023; Hollaar et al., 2023; Korte et al., 2015; Merkel & Munnecke, 2023).

The main changes in observed sedimentary mineralogy and detrital zircon ages correspond closely in timing to many of these major paleoclimatic and tectonic episodes. In the following section we consider the possible mechanisms by which these environmental factors affected depositional processes and defined the observed mineral assemblages.

4.3. Mineral Assemblage Unit Characteristics, Provenance and Paleoenvironmental Change

Mineral Assemblage Unit 2, belonging to the middle to upper Sinemurian is characterized by low carbonate content, high feldspar to quartz ratios in the major detrital grains, high biotite content and detrital zircons that are predominantly pre-Cadomian in age (Figure 5). Most zircons older than about 950 Ma will have been derived from Laurentia and the deformed Laurentian margin (Figure 1), thus the zircon age spectra indicate an ultimate provenance from the north (cf. Cawood, Nemchin, et al., 2003; Johansson et al., 2022; Johnson et al., 2016; Morton et al., 2021). Although we have few data, it appears that Mineral Assemblage Unit 1, comprising the Hettangian and lowest Sinemurian, has overall similar characteristics and provenance (Figure 2). The strongly feldspathic nature of the sediment, particularly the abundance of albite, indicates relatively un-weathered and first-cycle source materials.

It is difficult to fully exclude the possibility that the zircons have been recycled through a younger sedimentary succession such as Upper Paleozoic strata that may originally have overlain Lower Paleozoic rocks now forming the bulk of the Welsh Massif (e.g., Cope, 1984). However, it is clear that assemblages 1 and 2 contain far fewer grains of Caledonian or Cadomian origins than the overlying units, and thus we interpret the overall pattern to indicate greater preponderance of zircons ultimately derived from the north. If the overall stratigraphic patterns observed through the whole core represent an unroofing stratigraphy, it is clear the unroofed succession contained very systematically distributed zircon-age populations with an ordering that was preserved (albeit inversely) during the erosion process occurring over some 20 million years of Early Jurassic time. Good preservation of a purely reworked signal in consistent stratigraphic trends appears to us to be a much less likely explanation for the observations than overall change in provenance direction through the Early Jurassic. This is especially the case because there is no evidence that an unroofed succession would anyway have a predominance of reworked pre-Cadomian grains at the top and a predominance of Cadomian grains at the base; the only clear evidence that we have, from the Carboniferous sandstones of the Pennine Basin (Morton et al., 2021), would have led to an ordering opposite to that observed.

Assemblage Unit 3, belonging to the uppermost Sinemurian ammonite chronozone (Raricostatum) is quite distinctive in its detrital zircon population, comprising predominantly Caledonian grains, although its major detrital mineralogy is intermediate between the underlying and overlying strata and retains a strong feldspar component (Figure 5). The depositional site is directly adjacent to the Megumia and Ganderia terranes (Figure 2) that were strongly deformed in the Caledonian Orogeny, suggesting that this part of the succession has a strong locally sourced component, and we also note that these terranes would also have imparted a Cadomian signature to the derived sediments (Fairey et al., 2018).

The Pliensbachian Assemblage Unit 4 shows a step change increase in Cadomian-age zircons, whilst also showing a substantial reduction in abundance of Caledonian aged grains. Overall, the detrital grains are quartz-dominated; albite disappears from the assemblages, and K-feldspar content is low except at the very top of the unit. This change in mineral assemblage indicates a significant change in sediment sources that coincides with major relative (possibly global) sea-level rise in concert with the Sinemurian–Pliensbachian boundary event. The coincidence suggests a reorganization of sediment dispersal systems across the region. The switch to grains with an ultimate southern peri-Gondwanan Late Proterozoic (Cryogenian and late Ediacaran) source points toward the establishment of bottom currents from the south or west in the earliest Pliensbachian and thus a reversal from the previous state. As described in Section 4.2 above, this inferred change co-occurs with the modeled reversal in seaway flow in the SW Laurasian Seaway that accompanies the opening of the Hispanic corridor (Ruvalcaba Baroni et al., 2018). We therefore suggest that the observed mineralogical changes occurring across the Sinemurian–Pliensbachian transition are controlled largely by this major tectonic and paleoceanographic event. In conjunction, extensional tectonics occurred west of Iberia, opening up N-S oriented seaways in the Lusitanian, Peniche and Galicia Interior basins, improving connectivity to Tethys of more northerly basins such as the Cardigan Bay Basin (Walker et al., 2021). Moreover, regional relative sea-level rise at the beginning of the Pliensbachian would have increased the cross-sectional area of all the seaways in the region, again facilitating greater throughflow of water masses derived from equatorial Tethys (Section 4.2, Figure 5).

Whilst the grain size becomes distinctively coarser through Unit 4 (the bulk of the Pliensbachian Stage)—similar to patterns of coarsening in adjacent sedimentary basins (Hesselbo, 2008)—the detrital zircon ages hardly change. This observation is compatible with the interpretation of Pieńkowski et al. (2021) that grain size in the Mochras core reflects principally variations in contour current strength in the marine strait, rather than localized change in sediment sources. Relative sea-level fall on the basin margins may at the same time have been responsible for delivery of coarser sediment into the deep-water transport and depositional systems, with the two effects working in concert. Our results are seemingly at odds with those of Dera et al. (2009) who suggested, on the basis of Nd isotopes in fish teeth from the Paris Basin and Worcester Graben, that the water mass flow through the Laurasian Seaway was north-to-south except in the latest Pliensbachian; however, we note that the reported isotope data are very sparse and the crustal Nd isotope values would not be expected to distinguish source terrains in the region to the same degree as the zircon age data.

Lastly, the base of Unit 5 represents a second step change toward dominance of Cadomian zircon grains (southerly or westerly sources) with only residual proportions of either Caledonian or pre-Cadomian grains. This change in zircon age spectra takes place alongside a transition through the top Pliensbachian and base Toarcian toward much finer grained more micaceous mudstone containing little carbonate. Our major mineral data set does not go higher than the middle Toarcian, but based on visual core description, the upper Toarcian is characterized by coarsening in a very similar manner to the pattern observed for the Pliensbachian. Zircon age spectra continue to be dominated by Cadomian grains to the top of the Toarcian section. The interpretation suggested here is that the configuration of sediment transport from the south established in the Pliensbachian is maintained and strengthened in the Toarcian.

The Pliensbachian–Toarcian transition, like the Sinemurian–Pliensbachian transition before, was a time of major global sea-level rise, and the transition from a late Pliensbachian “Cool Mode” or even “Icehouse” (Figure 5; Korte & Hesselbo, 2011; Merkel & Munnecke, 2023; Nordt et al., 2022; Price, 1999; Rogov & Zakharov, 2010; Ruebsam & Schwark, 2021; Ruebsam et al., 2019) to the early Toarcian super-Greenhouse conditions manifest as the T-OAE (e.g., Dera et al., 2011; Jenkyns, 1988, 2010; Suan et al., 2010). It is particularly notable that detrital zircon age spectra maintain largely the same characteristics despite the marked change in other sedimentary grain properties (Figures 2, 3 and 5). This suggests that contrary to previous interpretations (Bjerrum et al., 2001; Dera & Donnadieu, 2012; Pieńkowski et al., 2024) the major global paleoclimatic events in the early Toarcian may have had relatively little impact in the pattern of water mass flows through the Laurasian Seaway. With respect to the T-OAE, Xu et al. (2018) suggested enhanced turbidite deposition, evident as discrete very fine sand beds derived from the local basin margins as a result of greatly increased rainfall; our data currently do not have sufficient resolution and stratigraphic precision to test this hypothesis, but such local derivation may explain the spikiness (i.e., high fluctuations defined by single sample points) seen in our data for the OAE, as well as the abundance of plant fossils (Figures 2 and 5).

5. Conclusions

The Lower Jurassic succession at Mochras (Cardigan Bay Basin), deposited in a silty argillaceous hemipelagic deep water setting, comprises five mineral assemblage units based upon major and minor mineralogical compositions and detrital zircon provenance data. The mineral assemblage unit boundaries correspond to times of major paleoenvironmental change including both sea-level rise and episodes of regional or global warming. These transitions also lie close to or coincide with the Early Jurassic stage boundaries.

Detrital zircon age frequency data show clear changes in ultimate provenance, shifting from pre-Cadomian (>900 Ma) in Unit 1 and Unit 2 (Hettangian and Sinemurian), Caledonian (490–390 Ma) dominance (briefly) in Unit 3 (uppermost Sinemurian), to Cadomian (750–540 Ma) dominance in Unit 4 (Pliensbachian) and, especially, Unit 5 (Toarcian). We interpret this pattern of change to correspond to a shift from northern provenance during the Hettangian and most of the Sinemurian, to more localized derivation in the latest Sinemurian, and southern and western dominance during the Pliensbachian and Toarcian. The observed trends and shifts are interpreted as a response primarily to a systematic change in sediment transport paths in the meridional Laurasian Seaway, with earlier southward flow switching to northward flow through the Early Jurassic, first at the beginning of the Pliensbachian and then strengthened at the start of the Toarcian.

We hypothesize that this overall shift in transport direction in the Cardigan Bay Basin relates principally to opening of the Hispanic Corridor around the time of the Sinemurian–Pliensbachian boundary, with ongoing "Central Atlantic" rifting and global sea-level rise also playing supplemental roles. Further factors influencing the details of sedimentary mineralogy include relative sea-level change and regional climate; relative sea-level lowstand and associated semi-arid climate delivered sediment to the basin exhibiting significantly lower mineralogical maturity than occurred during sea-level highstand and associated humid climate states.

Conflict of Interest

The authors declare no conflicts of interest relevant to this study.

Availability Statement

Data are fully available from the UK National Geoscience Data Centre: Jiang et al. (2026a), Quantitative mineralogy from the Lower Jurassic of the Llanbedr (Mochras Farm) borehole, Wales; Jiang et al. (2026b), Detrital zircon U-Pb ages from the Lower Jurassic of the Llanbedr (Mochras Farm) borehole, Wales.

Acknowledgments
MJ acknowledges funding from the China Scholarship Council (201806410016). SPH and CVU were supported through NERC grant NE/N018508/1. Work by GP, EK, AU and DS is financed by the National Science Centre, Poland, from the programme Opus 13, Grant Agreement No. 2017/25/B/ST10/02235. This is a contribution to the International Continental Scientific Drilling Program (ICDP) project: Early Jurassic Earth System and Timescale (JET). We thank staff at the UK National Core Repository, BGS, Nottingham, UK for support over many years. JBR publishes with the approval of the Director, BGS (NERC). We thank reviewers Michael Pointon and Emanuela Mattioli for their critical insights on the draft manuscript. Gavyn Rollinson (University of Exeter) is thanked for advice on quantitative mineralogy.

References

Aberhan, M. (2001). Bivalve palaeobiogeography and the Hispanic Corridor: Time of opening and effectiveness of a proto-Atlantic seaway. *Palaeogeography, Palaeoclimatology, Palaeoecology*, *165*(3–4), 375–394. https://doi.org/10.1016/S0031-0182(00)00172-3

Aberhan, M. (2002). Opening of the Hispanic Corridor and the Early Jurassic bivalve biodiversity. In J. A. Crame & A. W. Owen (Eds.), *Palaeobiogeography and biodiversity change: The ordovician and mesozoic-cenozoic radiations. Geological Society London Special Publications* (Vol. 194, pp. 127–139). https://doi.org/10.1144/GSL.SP.2002.194.01.10

Ambrose, K. (2001). The lithostratigraphy of the Blue Lias Formation (late Rhaetian–early Sinemurian) in the southern part of the English Midlands. *Proceedings of the Geologists' Association*, *112*(2), 97–110. https://doi.org/10.1016/S0016-7878(01)80020-1

Archer, S. G., Steel, R. J., Mellere, D., Blackwood, S., & Cullen, B. (2019). Response of Middle Jurassic shallow-marine environments to syn-depositional block tilting: Isles of Skye and Raasay, NW Scotland. *Scottish Journal of Geology*, *55*(1), 35–68. https://doi.org/10.1144/sjg2018-014

Arias, C. (2007). Pliensbachian–Toarcian ostracod biogeography in NW Europe: Evidence for water mass structure evolution. *Palaeogeography, Palaeoclimatology, Palaeoecology*, *251*(3–4), 398–421. https://doi.org/10.1016/j.palaeo.2007.04.014

Baghli, H., Mattioli, E., Spangenberg, J. E., Ruebsam, W., Schwark, L., Bensalah, M., et al. (2022). Stratification and productivity in the Western Tethys (NW Algeria) during early Toarcian. *Palaeogeography, Palaeoclimatology, Palaeoecology*, *591*, 110864. https://doi.org/10.1016/j.palaeo.2022.110864

Bjerrum, C. J., Surlyk, F., Callomon, J. H., & Slingerland, R. L. (2001). Numerical paleoceanographic study of the Early Jurassic transcontinental Laurasian seaway. *Paleoceanography*, *16*(4), 390–404. https://doi.org/10.1029/2000PA000512

Black, L. P., Kamo, S. L., Allen, C. M., Aleinikoff, J. N., Davis, D. W., Korsch, R. J., & Foudoulis, C. (2003). TEMORA 1: A new zircon standard for Phanerozoic U–Pb geochronology. *Chemical Geology*, *200*(1–2), 155–170. https://doi.org/10.1016/S0009-2541(03)00165-7

Bodin, S., Fantasia, A., Krencker, F.-N., Nebsbjerg, B., Christiansen, L., & Andrieu, S. (2023). More gaps than record! A new look at the Pliensbachian/Toarcian boundary event guided by coupled chemo-sequence stratigraphy. *Palaeogeography, Palaeoclimatology, Palaeoecology*, *610*, 111344. https://doi.org/10.1016/j.palaeo.2022.111344

Casas, J. M., & Murphy, J. B. (2018). Unfolding the arc: The use of pre-orogenic constraints to assess the evolution of the Variscan belt in Western Europe. *Tectonophysics*, *736*, 47–61. https://doi.org/10.1016/j.tecto.2018.04.012

Cawood, P. A., Hawkesworth, C. J., & Dhuime, B. (2012). Detrital zircon record and tectonic setting. *Geology*, *40*(10), 875–878. https://doi.org/10.1130/G32945.1

Cawood, P. A., Nemchin, A. A., Freeman, M., & Sircombe, K. (2003). Linking source and sedimentary basin: Detrital zircon record of sediment flux along a modern river system and implications for provenance studies. *Earth and Planetary Science Letters*, *210*(1–2), 259–268. https://doi.org/10.1016/S0012-821X(03)00122-5

Cawood, P. A., Nemchin, A. A., Strachan, R., Prave, T., & Krabbendam, M. (2007). Sedimentary basin and detrital zircon record along East Laurentia and Baltica during assembly and breakup of Rodinia. *Journal of the Geological Society*, *164*(2), 257–275. https://doi.org/10.1144/0016-76492006-115

Cawood, P. A., Nemchin, A. A., Strachan, R. A., Kinny, P. D., & Loewy, S. (2004). Laurentian provenance and an intracratonic tectonic setting for the Moine Supergroup, Scotland, constrained by detrital zircons from the Loch Eil and Glen Urquhart successions. *Journal of the Geological Society*, *161*(5), 861–874. https://doi.org/10.1144/16-764903-117

Cawood, P. A., Nemchin, A. A., Smith, M., & Loewy, S. (2003). Source of the Dalradian Supergroup constrained by U-Pb dating of detrital zircons and implications for the East Laurentian margin. *Journal of the Geological Society*, *160*(2), 231–246. https://doi.org/10.1144/0016-764902-039

Chadwick, R. A., & Evans, D. J. (2005). A seismic Atlas of Southern Britain – Images of subsurface structure. *British Geological Survey Occasional Publications*, *7*, 1–196. Retrieved from https://nora.nerc.ac.uk/id/eprint/11482/

Chew, D. M., O'Sullivan, G., Caracciolo, L. M. C., & Tyrrell, S. (2020). Sourcing the sand: Accessory mineral fertility, analytical and other biases in detrital U-Pb provenance analysis. *Earth-Science Reviews*, *202*, 103093. https://doi.org/10.1016/j.earscirev.2020.103093

Chew, D. M., & Stillman, C. J. (2009). Late Caledonian Orogeny and magmatism. In C. H. Holland & I. S. Sanders (Eds.), *The Geology of Ireland* (pp. 143–174). Liverpool University Press. https://doi.org/10.2307/jj.12638997.11

Chew, D. M., & Strachan, R. A. (2014). *The Laurentian Caledonides of Scotland and Ireland*. Geological Society of London Special Publications, (Vol. 390(1), pp. 45–91). https://doi.org/10.1144/SP390.16

Clarke, A. J., Kirkland, C. L., Bevins, R. E., Pearce, N. J., Glorie, S., & Ixer, R. A. (2024). A Scottish provenance for the Altar Stone of Stonehenge. *Nature*, *632*(8025), 570–575. https://doi.org/10.1038/s41586-024-07652-1

Condie, K. C., & Aster, R. C. (2010). Episodic zircon age spectra of orogenic granitoids: The supercontinent connection and continental growth. *Precambrian Research*, *180*(3–4), 227–236. https://doi.org/10.1016/j.precamres.2010.03.008

Cope, J. C. W. (1984). The Mesozoic history of Wales. *Proceedings of the Geological Association*, *95*(4), 373–385. https://doi.org/10.1016/S0016-7878(84)80067-X

Cope, J. C. W. (1995). Introduction to the British Jurassic. In P. D. Taylor (Ed.), *Field Geology of the British Jurassic* (pp. 1–7). Geological Society of London, Bath.

Cope, J. C. W., Getty, T. A., Howarth, M. K., Morton, N., & Torrens, H. S. (1980). A correlation of Jurassic rocks in the British Isles. Part one: Introduction and Lower Jurassic. *Geological Society of London, Special Report*, *14*, 1–73.

Copestake, P., & Johnson, B. (2014). Lower Jurassic Foraminifera from the Llanbedr (Mochras Farm) borehole, North Wales, UK. *Monograph of the Palaeontological Society*, *167*(641), 1–403. https://doi.org/10.1080/02693445.2013.11963952

Copestake, P., & Partington, M. A. (2023). Sequence stratigraphy of the Jurassic–Lowermost Cretaceous (Hettangian–Berriasian) of the North Sea Region. *Geological Society*, *59*(1), 65–97. https://doi.org/10.1144/M59-2022-67

Cox, B. M., Sumbler, M. G., & Ivimey-Cook, H. C. (1999). A formational framework for the Lower Jurassic of England and Wales (onshore area). *British Geological Survey Research Report, RR/99/01*, 1–28.

Damborenea, S. E., Echevarría, J., & Ros-Franch, S. (2013). Southern Hemisphere palaeobiogeography of Triassic-Jurassic marine bivalves. In *Springer briefs, seaways and landbridges: Southern Hemisphere biogeographic connections through time* (p. 139). Springer. https://doi.org/10.1007/978-94-007-5098-2_1

Danisch, J., Kabiri, L., Nutz, A., & Bodin, S. (2019). Chemostratigraphy of late Sinemurian – Early Pliensbachian shallow-to deep-water deposits of the Central High Atlas Basin: Paleoenvironmental implications. *Journal of African Earth Sciences*, *153*, 239–249. https://doi.org/10.1016/j.jafrearsci.2019.03.003

Deconinck, J. F., Hesselbo, S. P., & Pellenard, P. (2019). Climatic and sea-level control of Jurassic (Pliensbachian) clay mineral sedimentation in the Cardigan Bay Basin, Llanbedr (Mochras Farm) borehole Wales. *Sedimentology*, *66*(7), 2769–2783. https://doi.org/10.1111/sed.12610

de Graciansky, P.-C., Jacquin, T., & Hesselbo, S. P. (1998). *The Ligurian cycle: An overview of Lower Jurassic 2nd-order transgressive/regressive facies cycles in Western Europe* (Vol. 60, pp. 467–480). SEPM Special Publication. https://doi.org/10.2110/pec.98.02.0467

Dera, G., & Donnadieu, Y. (2012). Modeling evidences for global warming, Arctic seawater freshening, and sluggish oceanic circulation during the Early Toarcian anoxic event. *Paleoceanography*, *27*(2), PA2211. https://doi.org/10.1029/2012PA002283

Dera, G., Neige, P., Dommergues, J.-L., & Brayard, A. (2011). Ammonite paleobiogeography during the Pliensbachian–Toarcian crisis (Early Jurassic) reflecting paleoclimate, eustasy, and extinctions. *Global and Planetary Change*, *78*(3–4), 92–105. https://doi.org/10.1016/j.gloplacha.2011.05.009

Dera, G., Pucéat, E., Pellenard, P., Neige, P., Delsate, D., Joachimski, M. M., et al. (2009). Water mass exchange and variations in seawater temperature in the NW Tethys during the Early Jurassic: Evidence from neodymium and oxygen isotopes of fish teeth and belemnites. *Earth and Planetary Science Letters*, *286*(1–2), 198–207. https://doi.org/10.1016/j.epsl.2009.06.027

Dercourt, J., Gaetani, M., Vrielynck, B., Barriere, E., Biju-Duval, B., Brunet, M.-F., et al. (Eds.) (2000). *Atlas Peri-Tethys, Palaeogeographical maps* (pp. 1–269). CCGM/CGMW, Paris: 24 maps and explanatory notes: I–XX.

Dickinson, W. (2008). Impact of differential zircon fertility of granitoid basement rocks in North America on age populations of detrital zircons and implications for granite petrogenesis. *Earth and Planetary Science Letters*, *275*(1–2), 80–92. https://doi.org/10.1016/j.epsl.2008.08.003

Dobson, M. R., & Whittington, R. J. (1987). The geology of Cardigan Bay. *Proceedings of the Geologists' Association*, *98*(4), 331–353. https://doi.org/10.1016/S0016-7878(87)80074-3

Duarte, L. V., Comas-Rengifo, M. J., Silva, R. L., Paredes, R., & Goy, A. (2014). Carbon isotope stratigraphy and ammonite biochronostratigraphy across the Sinemurian-Pliensbachian boundary in the western Iberian margin. *Bulletin of Geosciences*, *89*(4), 719–773. https://doi.org/10.3140/bull.geosci.1476

Fairey, B. J., Aidan Kerrison, A., Meere, P. A., Mulchrone, K. F., Hofmann, M., Gärtner, A., et al. (2018). The provenance of the Devonian Old Red Sandstone of the Dingle Peninsula, SW Ireland; the earliest record of Laurentian and peri-Gondwanan sediment mixing in Ireland. *Journal of the Geological Society*, *175*(3), 411–424. https://doi.org/10.1144/jgs2017-099

Fedo, C. M., Sircombe, K. N., & Rainbird, R. H. (2003). Detrital zircon analysis of the sedimentary record. *Reviews in Mineralogy and Geochemistry*, *53*(1), 277–303. https://doi.org/10.2113/0530277

Fendley, I. M., Frieling, J., Mather, T. A., Ruhl, M., Hesselbo, S. P., & Jenkyns, H. C. (2024). Quantifying Early Jurassic Large Igneous Province carbon emissions via sedimentary mercury. *Nature Geoscience*, *17*(3), 241–248. https://doi.org/10.1038/s41561-024-01378-5

Ferreira, J., Mattioli, E., Sucherás-Marx, B., Giraud, F., Duarte, L. V., Pittet, B., et al. (2019). Western Tethys Early and Middle Jurassic calcareous nannofossil biostratigraphy. *Earth-Science Reviews*, *197*(2019), 102908. https://doi.org/10.1016/j.earscirev.2019.102908

Folk, R. L., & Ward, W. C. (1957). A study in the significance of grain-size parameters. *Journal of Sedimentary Petrology*, *27*(1), 3–26. https://doi.org/10.1306/74D70646-2B21-11D7-8648000102C1865D

Franceschi, M., Jin, X., Shi, Z., Chen, B., Preto, N., Roghi, G., et al. (2023). High-resolution record of multiple organic carbon-isotope excursions in lacustrine deposits of Upper Sinemurian through Pliensbachian (Early Jurassic) from the Sichuan Basin, China. *Geological Society of America Bulletin*, *135*(1–2), 3–17. https://doi.org/10.1130/b36235.1

Garzanti, E. (2016). From static to dynamic provenance analysis – Sedimentary petrology upgraded. *Sedimentary Geology*, *336*, 3–13. https://doi.org/10.1016/j.sedgeo.2015.07.010

Gehrels, G. (2012). Detrital zircon U-Pb geochronology: Current methods and new opportunities. In C. Busby & A. Azor (Eds.), *Tectonics of sedimentary basins: Recent advances* (pp. 45–62). Wiley-Blackwell. https://doi.org/10.1002/9781444347166.ch2

Hallam, A. (1969). Tectonism and eustasy in the Jurassic. *Earth-Science Reviews*, *5*(1), 45–68. https://doi.org/10.1016/0012-8252(69)90051-8

Hallam, A. (1981). A revised sea-level curve for the Early Jurassic. *Journal of the Geological Society*, *138*(6), 735–743. https://doi.org/10.1144/gsjgs.138.6.0735

Hallam, A. (2001). A review of the broad pattern of Jurassic sea-level changes and their possible causes in the light of current knowledge. *Palaeogeography, Palaeoclimatology, Palaeoecology*, *167*(1–2), 23–37. https://doi.org/10.1016/S0031-0182(00)00229-7

Hallsworth, C. R., Morton, A. C., Claoué-Long, J., & Fanning, C. M. (2000). Carboniferous sand provenance in the Pennine Basin, UK: Constraints from heavy mineral and detrital zircon age data. *Sedimentary Geology*, *137*(3–4), 147–185. https://doi.org/10.1016/S0037-0738(00)00153-6

Haq, B. (2017). Jurassic sea-level variations: A reappraisal. *GSA Today*, *28*, 7–10. https://doi.org/10.1130/GSATG359A.1

Hawkesworth, C. J., Dhuime, B., Pietranik, A. B., Cawood, P. A., Kemp, A. I., & Storey, C. D. (2010). The generation and evolution of the continental crust. *Journal of the Geological Society*, *167*(2), 229–248. https://doi.org/10.1144/0016-76492009-072

Hesselbo, S. P. (2008). Sequence stratigraphy and inferred relative sea-level change from the onshore British Jurassic. *Proceedings of the Geologists' Association*, *119*(1), 19–34. https://doi.org/10.1016/S0016-7878(59)80069-9

Hesselbo, S. P. (2012). Late Triassic–Jurassic: Disintegrating Pangaea. In N. H. Woodcock & R. A. Strachan (Eds.), *Geological History of Britain and Ireland* (2nd ed.). Blackwell. https://doi.org/10.1002/9781118274064.ch17

Hesselbo, S. P., Al-Suwaidi, A., Baker, S. J., Ballabio, G., Belcher, C. M., Bond, A., et al. (2023). Initial results of coring at Prees, Cheshire Basin, UK (ICDP JET Project); towards an integrated stratigraphy, timescale, and Earth system understanding for the Early Jurassic. *Scientific Drilling*, *32*, 1–25. https://doi.org/10.5194/sd-32-1-2023

Hesselbo, S. P., Bjerrum, C. J., Hinnov, L. A., MacNiocaill, C., Miller, K. G., Riding, J. B., & van de Schootbrugge, B. (2013). Mochras borehole revisited: A new global standard for Early Jurassic Earth history. *Scientific Drilling*, *16*, 81–91. https://doi.org/10.5194/sd-16-81-2013

Hesselbo, S. P., Gröcke, D. R., Jenkyns, H. C., Bjerrum, C. J., Farrimond, P. L., Morgans-Bell, H. S., & Green, O. (2000). Massive dissociation of gas hydrates during a Jurassic Oceanic Anoxic Event. *Nature*, *406*(6794), 392–395. https://doi.org/10.1038/35019044

Hesselbo, S. P., Hudson, A. J. L., Huggett, J. M., Leng, M. J., Riding, J. B., & Ullmann, C. V. (2020). Palynological, geochemical, and mineralogical characteristics of the Early Jurassic Liasidium Event in the Cleveland Basin, Yorkshire, UK. *Newsletters on Stratigraphy*, *53*(2), 191–211. https://doi.org/10.1127/nos/2019/0536

Hesselbo, S. P., & Jenkyns, H. C. (1998). British Lower Jurassic sequence stratigraphy. In P. C. De Graciansky, J. Hardenbol, T. Jacquin, & P. R. Vail (Eds.), *Mesozoic and Cenozoic sequence stratigraphy of European basins* (Vol. 60, pp. 561–581). SEPM Special Publication. https://doi.org/10.2110/pec.98.02.0561

Hesselbo, S. P., Jenkyns, H. C., Duarte, L. V., & Oliveira, L. C. V. (2007). Carbon-isotope record of the Early Jurassic (Toarcian) Oceanic Anoxic Event from fossil wood and marine carbonate (Lusitanian Basin, Portugal). *Earth and Planetary Science Letters*, *253*(3–4), 455–470. https://doi.org/10.1016/j.epsl.2006.11.009

Hesselbo, S. P., Korte, C., Ullmann, C. V., & Ebbesen, A. (2020). Carbon and oxygen isotope records from the southern Eurasian Seaway following the Triassic-Jurassic boundary: Parallel long-term enhanced carbon burial and seawater warming. *Earth-Science Reviews*, *203*, 103131. https://doi.org/10.1016/j.earscirev.2020.103131

Hesselbo, S. P., Robinson, S. A., & Surlyk, F. (2004). Sea-level change and facies development across potential Triassic–Jurassic boundary horizons, SW Britain. *Journal of the Geological Society*, *161*, 365–379. https://doi.org/10.1144/0016-764904-069

Hollaar, T. P., Baker, S. J., Hesselbo, S. P., Deconinck, J.-F., Mander, L., Ruhl, M., & Belcher, C. M. (2021). Wildfire activity enhanced during phases of maximum orbital eccentricity and precessional forcing in the Early Jurassic. *Communications Earth & Environment*, *2*(1), 247. https://doi.org/10.1038/s43247-021-00307-3

Hollaar, T. P., Hesselbo, S. P., Deconinck, J.-F., Damaschke, M., Ullmann, C. V., Jiang, M., & Belcher, C. M. (2023). Environmental changes during the onset of the Late Pliensbachian Event (Early Jurassic) in the Cardigan Bay Basin, Wales. *Climate of the Past*, *19*(5), 979–997. https://doi.org/10.5194/cp-19-979-2023

Hudson, A. J. L., Hesselbo, S. P., Hinnov, L. A., Littler, K., Page, K. N., Riding, J. B., et al. (2025). Astrochronology of the Sinemurian Stage from the Llanbedr (Mochras Farm) core, NW Wales: Implications for the Early Jurassic timescale. *Volumina Jurassica*, *23*, 43–64. https://doi.org/10.7306/VJ.23.2

Jenkyns, H. C. (1988). The early Toarcian (Jurassic) anoxic event: Stratigraphic, sedimentary, and geochemical evidence. *American Journal of Science*, *288*(2), 101–151. https://doi.org/10.2475/ajs.288.2.101

Jenkyns, H. C. (2010). Geochemistry of oceanic anoxic events. *Geochemistry, Geophysics, Geosystems*, *11*(3), 1–30. https://doi.org/10.1029/2009GC002788

Jenkyns, H. C., Jones, C. E., Gröcke, D. R., Hesselbo, S. P., & Parkinson, D. N. (2002). Chemostratigraphy of the Jurassic System: Applications, limitations and implications for palaeoceanography. *Journal of the Geological Society*, *159*(4), 351–378. https://doi.org/10.1144/0016-764901-130

Jiang, M., Hesselbo, S. P., Pieńkowski, G., Krzemińska, E., Riding, J. B., Uchman, A., et al. (2026a). Quantitative mineralogy from the Lower Jurassic of the Llanbedr (Mochras Farm) borehole, Wales [Dataset]. *National Geoscience Data Centre*. https://doi.org/10.5285/8ac36eba-6e5c-4ea4-bda8-f3b7d570018e

Jiang, M., Hesselbo, S. P., Pieńkowski, G., Krzemińska, E., Riding, J. B., Uchman, A., et al. (2026b). Detrital zircon U-Pb ages from the Lower Jurassic of the Llanbedr (Mochras Farm) borehole, Wales [Dataset]. *National Geoscience Data Centre*. https://doi.org/10.5285/386344e4-b0bf-4014-92a3-1f11c0ef2e3a

Johansson, Å., Bingen, B., Huhma, H., Waight, T., Vestergaard, R., Soesoo, A., et al. (2022). A geochronological review of magmatism along the external margin of Columbia and in the Grenville-age orogens forming the core of Rodinia. *Precambrian Research*, *371*, 106463. https://doi.org/10.1016/j.precamres.2021.106463

Johnson, T. E., Kirkland, C. L., Reddy, S. M., Evans, N. J., & McDonald, B. J. (2016). The source of Dalradian detritus in the Buchan Block, NE Scotland: Application of new tools to detrital datasets. *Journal of the Geological Society*, *173*(5), 773–782. https://doi.org/10.1144/jgs2016-019

Korte, C., & Hesselbo, S. P. (2011). Shallow marine carbon and oxygen isotope and elemental records indicate icehouse-greenhouse cycles during the Early Jurassic. *Paleoceanography*, *26*(4), PA4219. https://doi.org/10.1029/2011PA002160

Korte, C., Hesselbo, S. P., Ullmann, C. V., Dietl, G., Ruhl, M., Schweigert, G., & Thibault, N. R. (2015). Jurassic climate mode governed by ocean gateway. *Nature Communications*, *6*(1), 10015. https://doi.org/10.1038/ncomms10015

Košler, J., Fonneland, H., Sylvester, P., Tubrett, M., & Pedersen, R.-B. (2002). U-Pb dating of detrital zircons for sediment provenance studies – A comparison of laser ablation ICPMS and SIMS techniques. *Chemical Geology*, *182*(2–4), 605–618. https://doi.org/10.1016/S0009-2541(01)00341-2

Krabbendam, M., Bonsor, H., Horstwood, M. S., & Rivers, T. (2017). Tracking the evolution of the Grenvillian foreland basin: Constraints from sedimentology and detrital zircon and rutile in the Sleat and Torridon groups, Scotland. *Precambrian Research*, *295*, 67–89. https://doi.org/10.1016/j.precamres.2017.04.027

Lancaster, P. J., Daly, J. S., Storey, C. D., & Morton, A. C. (2017). Interrogating the provenance of large river systems: Multi-proxy *in situ* analyses in the Millstone Grit, Yorkshire. *Journal of the Geological Society*, *174*(1), 75–87. https://doi.org/10.1144/jgs2016-069

Landing, E., Keppie, J. D., Keppie, D. F., Geyer, G., & Westrop, S. R. (2022). Greater Avalonia – Latest Ediacaran–Ordovician "peribaltic" terrane bounded by continental margin prisms ("Ganderia," Harlech Dome, Meguma): Review, tectonic implications, and paleogeography. *Earth-Science Reviews*, *224*, 103863. https://doi.org/10.1016/j.earscirev.2021.103863

Leary, R. J., Smith, M. E., & Umhoefer, P. (2020). Grain-size control on detrital zircon cycloprovenance in the late Paleozoic Paradox and Eagle basins, USA. *Journal of Geophysical Research: Solid Earth*, *125*(7), e2019JB019226. https://doi.org/10.1029/2019JB019226

Linnemann, U., D'Lemos, R., Drost, K., Jeffries, T., Gerdes, A., Romer, R. L., et al. (2008). Cadomian tectonics. In T. McCann (Ed.), *The Geology of Central Europe: Volume 1: Precambrian and Palaeozoic* (pp. 103–154). The Geological Society. https://doi.org/10.1144/CEV1P.3

Linnemann, U., Gerdes, A., Drost, K., & Buschmann, B. (2007). The continuum between Cadomian orogenesis and opening of the Rheic Ocean: Constraints from LA-ICP-MS U-Pb zircon dating and analysis of plate-tectonic setting (Saxo-Thuringian zone, northeastern Bohemian Massif, Germany). In U. Linnemann, D. Nance, P. Kraft, & G. Zulauf (Eds.), *The Evolution of the Rheic Ocean: From Avalonian-Cadomian active margin to Alleghenian-Variscan collision* (Vol. 423, pp. 61–96). Geological Society of America Special Paper. https://doi.org/10.1130/2007.2423(03)

Linnemann, U., Gerdes, A., Hofmann, M., & Marko, L. (2014). The Cadomian Orogen: Neoproterozoic to Early Cambrian crustal growth and orogenic zoning along the periphery of the West African Craton—Constraints from U–Pb zircon ages and Hf isotopes (Schwarzburg Antiform, Germany). *Precambrian Research*, *244*, 236–278. https://doi.org/10.1016/j.precamres.2013.08.007

Linnemann, U., Pereira, F., Jeffries, T. E., Drost, K., & Gerdes, A. (2008). The Cadomian Orogeny and the opening of the Rheic Ocean: The diachrony of geotectonic processes constrained by LA-ICP-MS U-Pb zircon dating (Ossa-Morena and Saxo-Thuringian Zones, Iberian and Bohemian Massifs). *Tectonophysics*, *461*(1–4), 21–43. https://doi.org/10.1016/j.tecto.2008.05.002

Ludwig, K. (2009). Errors of isotope ratios acquired by double interpolation. *Chemical Geology*, *268*(1–2), 24–26. https://doi.org/10.1016/j.chemgeo.2009.07.004

Ludwig, K. R. (2012). *Isoplot 3.75, A geochronological toolkit for Microsoft Excel* (Vol. 5, pp. 1–75). Berkeley Geochronology Center Special Publication. Retrieved from https://www.bgc.org/isoplot/8857ffdd-0794-4f29-a547-a23f863a1ffc

Mayall, M. J. (1981). The Late Triassic Blue Anchor Formation and the initial Rhaetian marine transgression in south-west Britain. *Geological Magazine*, *118*(4), 377–384. https://doi.org/10.1017/S0016756800032246

McElwain, J. C., Murphy, J. W., & Hesselbo, S. P. (2005). Changes in carbon dioxide during an oceanic anoxic event linked to intrusion into Gondwana coals. *Nature*, *435*, 479–483. https://doi.org/10.1038/nature03618

McKerrow, W. S., Mac Niocaill, C., & Dewey, J. F. (2000). The Caledonian Orogeny redefined. *Journal of the Geological Society*, *157*(6), 1149–1154. https://doi.org/10.1144/jgs.157.6.1149

Merkel, A., & Munnecke, A. (2023). Glendonite-bearing concretions from the upper Pliensbachian (Lower Jurassic) of South Germany: Indicators for a massive cooling in the European epicontinental sea. *Facies*, *69*(3), 10. https://doi.org/10.1007/s10347-023-00667-6

Moecher, D. P., & Samson, S. D. (2006). Differential zircon fertility of source terranes and natural bias in the detrital zircon record: Implications for sedimentary provenance analysis. *Earth and Planetary Science Letters*, *247*(3–4), 252–266. https://doi.org/10.1016/j.epsl.2006.04.035

Moecher, D. P., Zotto, S. C., & Samson, S. D. (2023). The critical role of recycling of post-Grenvillian, Neoproterozoic sediments for Phanerozoic Laurentian clastic systems: Evidence from detrital-zircon and monazite geochronology and textures. *Journal of Sedimentary Research*, *93*(2), 118–144. https://doi.org/10.2110/jsr.2022.054

Morton, A., Knox, R., & Frei, D. (2016). Heavy mineral and zircon age constraints on provenance of the Sherwood Sandstone Group (Triassic) in the eastern Wessex Basin, UK. *Proceedings of the Geologists' Association*, *127*(4), 514–526. https://doi.org/10.1016/j.pgeola.2016.06.001

Morton, A. C., Chisholm, J. I., & Frei, D. (2021). Provenance of Carboniferous sandstones in the central and southern parts of the Pennine Basin, UK: Evidence from detrital zircon ages. *Proceedings of the Yorkshire Geological Society*, *63*(3), pygs2020-010. https://doi.org/10.1144/pygs2020-010

Morton, N., Smith, M., Dodd, T., Panciroli, E., & Randles, T. (2025). Jurassic: Pangaea break-up and birth of the Atlantic Ocean. In M. Smith & R. A. Strachan (Eds.), *The geology of Scotland* (5th ed., pp. 379–412). Geological Society of London. https://doi.org/10.1144/GOS5-2023-8

Moyen, J.-F., Guy, A., Fiannacca, P., Janoušek, V., Villaseca, C., & Ayarza Arribas, P. (2025). Granites and the nature of the Variscan crust. *Elements*, *21*(6), 415–421. https://doi.org/10.2138/gselements.21.6.415

Munier, T., Deconinck, J. F., Pellenard, P., Hesselbo, S. P., Riding, J. B., Ullmann, C. V., et al. (2021). Million-year-scale alternation of warm–humid and semi-arid periods as a mid-latitude climate mode in the Early Jurassic (late Sinemurian, Laurasian Seaway). *Climate of the Past*, *17*(4), 1547–1566. https://doi.org/10.5194/cp-17-1547-2021

Nauton-Fourteu, M., Tyrrell, S., & Morton, A. (2021). Heavy mineral variations in mid-carboniferous deltaic sandstones: Records of a pre-depositional sediment history? *Depositional Record*, *7*(1), 52–63. https://doi.org/10.1002/dep2.128

Newell, A. J. (2018). Rifts, rivers and climate recovery: A new model for the Triassic of England. *Proceedings of the Geologists' Association*, *129*(3), 352–371. https://doi.org/10.1016/j.pgeola.2017.04.001

Nordt, L., Breecker, D., & White, J. (2022). Jurassic greenhouse ice-sheet fluctuations sensitive to atmospheric CO_2 dynamics. *Nature Geoscience*, *15*(1), 54–59. https://doi.org/10.1038/s41561-021-00858-2

Page, K. N. (2008). The evolution and geography of Jurassic ammonoids. *Proceedings of the Geologists' Association*, *119*(1), 35–57. https://doi.org/10.1016/S0016-7878(08)80257-X

Percival, L. M. E., Cohen, A. S., Davies, M. K., Dickson, A. J., Hesselbo, S. P., Jenkyns, H. C., et al. (2016). Osmium-isotope evidence for two pulses of increased continental weathering linked to Early Jurassic volcanism and climate change. *Geology*, *44*(9), 759–762. https://doi.org/10.1130/G37997.1

Pharaoh, T. (2018). The Anglo-Brabant massif: Persistent but enigmatic palaeo-relief at the heart of western Europe. *Proceedings of the Geologists' Association*, *129*(3), 278–328. https://doi.org/10.1016/j.pgeola.2018.02.009

Pieńkowski, G., Schudack, M. E., Bosák, P., Enay, R., Feldman-Olszewska, A., Golonka, J., et al. (2008). Jurassic. In T. McCann (Ed.), *The Geology of Central Europe Volume 2: Mesozoic and Cenozoic*. Geological Society of London. https://doi.org/10.1144/CEV2P.2

Pieńkowski, G., Uchman, A., Ninard, K., & Hesselbo, S. P. (2021). Ichnology, sedimentology, and orbital cycles in the hemipelagic Early Jurassic Laurasian Seaway (Pliensbachian, Cardigan Bay Basin, UK). *Global and Planetary Change*, *207*, 103648. https://doi.org/10.1016/j.gloplacha.2021.103648

Pieńkowski, G., Uchman, A., Ninard, K., Page, K. N., & Hesselbo, S. P. (2024). Early Jurassic extrinsic solar system dynamics versus intrinsic Earth processes: Toarcian sedimentation and benthic life in deep-sea contourite drift facies, Cardigan Bay Basin, UK. *Progress in Earth and Planetary Science*, *11*(1), 18. https://doi.org/10.1186/s40645-024-00612-3

Pointon, M., Cliff, R., & Chew, D. (2011). The provenance of Western Irish Namurian Basin sedimentary strata inferred using detrital zircon U–Pb LA-ICP-MS geochronology. *Geological Journal*, *47*(1), 77–98. https://doi.org/10.1002/gj.1335

Porter, S. J., Selby, D., Suzuki, K., & Gröcke, D. (2013). Opening of a trans-pangaean marine corridor during the Early Jurassic: Insights from osmium isotopes across the Sinemurian–Pliensbachian GSSP, Robin Hood's Bay, UK. *Palaeogeography, Palaeoclimatology, Palaeoecology*, *375*, 50–58. https://doi.org/10.1016/j.palaeo.2013.02.012

Pothier, H. D., Waldron, J. W. F., Schofield, D. I., & DuFrane, S. A. (2015). Peri-Gondwanan terrane interactions recorded in the Cambrian–Ordovician detrital zircon geochronology of North Wales. *Gondwana Research*, *28*(3), 987–1001. https://doi.org/10.1016/j.gr.2014.08.009

Price, G. D. (1999). The evidence and implications of polar ice during the Mesozoic. *Earth-Science Reviews*, *48*(3), 183–210. https://doi.org/10.1016/S0012-8252(99)00048-3

Rainbird, R. H., & Ernst, R. E. (2001). The sedimentary record of mantle-plume uplift. In: R. E. Ernst, & K. L. Buchan (Eds.), *Mantle plumes: Their identification through time* (pp. 227–246). Geological Society of America Special Papers. https://doi.org/10.1130/0-8137-2352-3.227

Reggiani, L., Mattioli, E., Pittet, B., Duarte, L. V., Veiga de Oliveira, L. C., & Comas-Rengifo, M. J. (2010). Pliensbachian (Early Jurassic) calcareous nannofossils from the Peniche section (Lusitanian Basin, Portugal): A clue for palaeoenvironmental reconstructions. *Marine Micropaleontology*, *75*(1–4), 1–16. https://doi.org/10.1016/j.marmicro.2010.02.002

Remírez, M. N., & Algeo, T. J. (2020). Carbon-cycle changes during the Toarcian (Early Jurassic) and implications for regional versus global drivers of the Toarcian oceanic anoxic event. *Earth-Science Reviews*, *209*, 103283. https://doi.org/10.1016/j.earscirev.2020.103283

Riding, J. B., Leng, M. J., Kender, S., Hesselbo, S. P., & Feist-Burkhardt, S. (2013). Isotopic and palynological evidence for a new Early Jurassic environmental perturbation. *Palaeogeography, Palaeoclimatology, Palaeoecology*, *374*, 16–27. https://doi.org/10.1016/j.palaeo.2012.10.019

Rogov, M. A., & Zakharov, V. A. (2010). Jurassic and Lower Cretaceous glendonite occurrences and their implication for Arctic paleoclimate reconstructions and stratigraphy. *Earth Science Frontiers*, *17*, 345–347.

Rossi, V. M., Longhitano, S. G., Olariu, C., & Chiocci, F. L. (2023). Straits and seaways: End members within the continuous spectrum of the dynamic connection between basins. *Geological Society*, *523*(1), 85–109. https://doi.org/10.1144/sp523-2022-159

Rubatto, D. (2017). Zircon: The metamorphic mineral. *Reviews in Mineralogy and Geochemistry*, *83*(1), 261–295. https://doi.org/10.2138/rmg.2017.83.9

Ruebsam, W., Mayer, B., & Schwark, L. (2019). Cryosphere carbon dynamics control early Toarcian global warming and sea level evolution. *Global and Planetary Change*, *172*, 440–453. https://doi.org/10.1016/j.gloplacha.2018.11.003

Ruebsam, W., & Schwark, L. (2021). Impact of north-hemispherical cryosphere on early Toarcian climate and environmental perturbation. In M. Reolid, E. Mattioli, L. V. Duarte, & W. Ruebsam (Eds.), *Carbon Cycle and Ecosystem Response to the Jenkyns Event in the Early Toarcian (Jurassic)*. Geological Society, London, Special Publications (Vol. 514(Iss. 1), pp. 359–385). https://doi.org/10.1144/SP514-2021-11

Ruhl, M., Hesselbo, S. P., Hinnov, L., Jenkyns, H. C., Xu, W., Storm, M. S., et al. (2016). Astronomical constraints on the duration of the Early Jurassic Pliensbachian Stage and global climatic fluctuations. *Earth and Planetary Science Letters*, *455*, 149–165. https://doi.org/10.1016/j.epsl.2016.08.038

Ruhl, M., Hesselbo, S. P., Jenkyns, H. C., Xu, W., Silva, R. L., Matthews, K. J., et al. (2022). Reduced plate movement controlled onset and timing of Early Jurassic (Toarcian) Karoo-Ferrar large igneous province volcanism and global environmental change. *Science Advances*, *8*(36), eabo0866. https://doi.org/10.1126/sciadv.abo0866

Ruvalcaba Baroni, I., Pohl, A., van Helmond, N. A. G. M., Papadomanolaki, N. M., Coe, A. L., Cohen, A. S., et al. (2018). Ocean circulation in the Toarcian (Early Jurassic): A key control on deoxygenation and carbon burial on the European shelf. *Paleoceanography and Paleoclimatology*, *33*(9), 994–1012. https://doi.org/10.1029/2018PA003394

Schneider, C. A., Rasband, W. S., & Eliceiri, K. W. (2012). NIH Image to ImageJ: 25 years of image analysis. *Nature Methods*, *9*(7), 671–675. https://doi.org/10.1038/nmeth.2089

Schöllhorn, I., Adatte, T., van de Schootbrugge, B., Houben, A., Charbonnier, G., Janssen, N., & Föllmi, K. B. (2020). Climate and environmental response to the break-up of Pangea during the Early Jurassic (Hettangian–Pliensbachian); the Dorset coast (UK) revisited. *Global and Planetary Change*, *185*, 103096. https://doi.org/10.1016/j.gloplacha.2019.103096

Sellwood, B. W. (1972). Regional environmental changes across a Lower Jurassic stage-boundary in Britain. *Palaeontology*, *15*, 125–157.

Sláma, J., & Pedersen, R. B. (2015). Zircon provenance of SW Caledonian phyllites reveals a distant Timanian sediment source. *Journal of the Geological Society*, *172*(4), 465–478. https://doi.org/10.1144/jgs2014-143

Stacey, J. S., & Kramers, J. D. (1975). An approximation of terrestrial lead isotope evolution by a two-stage model. *Earth and Planetary Science Letters*, *26*(2), 207–221. https://doi.org/10.1016/0012-821X(75)90088-6

Storm, M. S., Hesselbo, S. P., Jenkyns, H. C., Ruhl, M., Ullmann, C. V., Xu, W., et al. (2020). Orbital pacing and secular evolution of the Early Jurassic carbon cycle. *Proceedings of the National Academy of Sciences*, *117*(8), 3974–3982. https://doi.org/10.1073/pnas.1912094117

Strachan, R. A., Collins, A. S., Buchan, C., Nance, R. D., Murphy, J. B., & D'Lemos, R. S. D. (2007). Terrane analysis along a Neoproterozoic active margin of Gondwana: Insights from U-Pb zircon geochronology. *Journal of the Geological Society*, *164*(1), 57–60. https://doi.org/10.1144/0016-76492006-014

Suan, G., Mattioli, E., Pittet, B., Lécuyer, C., Suchéras-Marx, B., Duarte, L. V., et al. (2010). Secular environmental precursors to Early Toarcian (Jurassic) extreme climate changes. *Earth and Planetary Science Letters*, *290*(3–4), 448–458. https://doi.org/10.1016/j.epsl.2009.12.047

Surlyk, F. (1990). A Jurassic sea-level curve for East Greenland. *Palaeogeography, Palaeoclimatology, Palaeoecology*, *78*(1–2), 71–85. https://doi.org/10.1016/0031-0182(90)90205-L

Surlyk, F., Alsen, P., Bjerager, M., Dam, G., Engkilde, M., Hansen, C. F., et al. (2021). Jurassic stratigraphy of East Greenland. *GEUS Bulletin*, *46*. https://doi.org/10.34194/geusb.v46.6521

Svensen, H., Planke, S., Chevallier, L., Malthe-Sørenssen, A., Corfu, B., & Jamtveit, B. (2007). Hydrothermal venting of greenhouse gases triggering Early Jurassic global warming. *Earth and Planetary Science Letters*, *256*(3–4), 554–566. https://doi.org/10.1016/j.epsl.2007.02.013

Sylvester, P. J., Souders, A. K., & Liu, R. (2022). Significance of U-Pb detrital zircon geochronology for mudstone provenance. *Geology*, *50*, 670–675. https://doi.org/10.1130/G49684

Tappin, D. R., Chadwick, R. A., Jackson, A. A., Wingfield, R. T. R., & Smith, N. J. P. (1994). Geology of Cardigan Bay and the Bristol Channel, United Kingdom offshore. *Regional Report, British Geological Survey, HMSO*, 107.

Thibault, N., Ruhl, M., Ullmann, C. V., Korte, C., Kemp, D. B., Gröcke, D. R., & Hesselbo, S. P. (2018). The wider context of the Lower Jurassic Toarcian oceanic anoxic event in Yorkshire coastal outcrops, UK. *Proceedings of the Geologists' Association*, *129*(3), 372–391. https://doi.org/10.1016/j.pgeola.2017.10.007

Thomas, W. (2011). Detrital-zircon geochronology and sedimentary provenance. *Lithosphere*, *3*(4), 304–308. https://doi.org/10.1130/RF.L001.1

Ullmann, C. V., Szűcs, D., Jiang, M., Hudson, A. J. L., & Hesselbo, S. P. (2022). Geochemistry of macrofossil, bulk rock, and secondary calcite in the Early Jurassic strata of the Llanbedr (Mochras Farm) drill core, Cardigan Bay Basin, Wales, UK. *Journal of the Geological Society*, *179*(1), jgs2021-018. https://doi.org/10.1144/jgs2021-018

Underhill, J. R., & Partington, M. A. (1993). Jurassic thermal doming and deflation in the North Sea: Implications of the sequence stratigraphic evidence. *Geological Society, London, Petroleum Geology Conference Series*, *4*(1), 337–345. https://doi.org/10.1144/0040337

van Buchem, F. S. P., & Knox, R. W. O. B. (1998). Lower and Middle Jurassic depositional sequences of Yorkshire (UK). In P. C. de Graciansky, J. Hardenbol, T. Jacquin, M. Farley, & R. R. Vail (Eds.), *Mesozoic–Cenozoic sequence stratigraphy of European basins* (Vol. 60, pp. 545–559). SEPM Special Publication. https://doi.org/10.2110/pec.98.02.0545

van de Schootbrugge, B., Houben, A. J. P., Ercan, F. E. Z., Verreussel, R., Kerstholt, S., Janssen, N. M. M., et al. (2019). Enhanced Arctic-Tethys connectivity ended the Toarcian Oceanic Anoxic Event in NW Europe. *Geological Magazine*, *157*(10), 1593–1611. https://doi.org/10.1017/S0016756819001262

Vermeesch, P. (2021). On the treatment of discordant detrital zircon U–Pb data. *Geochronology*, *3*(1), 247–257. https://doi.org/10.5194/gchron-3-247-2021

Walker, O. A., Alves, T. M., Hesselbo, S. P., Pharaoh, T., Nuzzo, M., & Mattos, N. H. (2021). Significance of Upper Triassic to Lower Jurassic salt in the identification of palaeo-seaways in the North Atlantic. *Marine and Petroleum Geology*, *123*, 104705. https://doi.org/10.1016/j.marpetgeo.2020.104705

Warrington, G., Audley-Charles, M. G., Elliott, R. E., Evans, W. B., Ivimey-Cook, H. C., Kent, P., et al. (1980). A correlation of Triassic rocks in the British Isles. In *Geological Society of London, Special Report* (Vol. 13, p. 78).

Waters, C. N., Morton, A., & Frei, D. (2021). Interplay of southern, western, and northern sources during deposition of North Wales Carboniferous sandstones, determined from heavy minerals, mineral chemistry, and detrital zircon ages. *Geological Journal*, *56*(5), 2699–2719. https://doi.org/10.1002/gj.4063

Wiedenbeck, M., Hanchar, J. M., Peck, W. H., Sylvester, P., Valley, J., Whitehouse, M., et al. (2004). Further characterisation of the 91500 zircon crystal. *Geostandards and Geoanalytical Research*, *28*(1), 9–39. https://doi.org/10.1111/j.1751-908X.2004.tb01041.x

Williams, I. S. (1998). U-Th-Pb geochronology by ion microprobe. *Reviews in Economic Geology*, *7*, 1–35. https://doi.org/10.5382/Rev.07.01

Wood, A., & Woodland, A. W. (1968). Borehole at Mochras, west of Llanbedr, Merionethshire. *Nature*, *219*(5161), 1352–1354. https://doi.org/10.1038/2191352a0

Woodland, A. W. (Ed.) (1971). *The Llanbedr (Mochras Farm) Borehole*. Institute of Geological Science, 115. https://doi.org/10.5194/sd-16-81-2013

Xu, W., Ruhl, M., Jenkyns, H. C., Leng, M. J., Huggett, J. M., Minisini, D., et al. (2018). Evolution of the Toarcian (Early Jurassic) carbon-cycle and global climatic controls on local sedimentary processes (Cardigan Bay Basin, UK). *Earth and Planetary Science Letters*, *484*, 396–411. https://doi.org/10.1016/j.epsl.2017.12.037

Yakymchuk, C., Kirkland, C. L., & Clark, C. (2018). Th/U ratios in metamorphic zircon. *Journal of Metamorphic Geology*, *36*(6), 715–737. https://doi.org/10.1111/jmg.12307

Ziegler, P. A. (1990). *Geological Atlas of Western and Central Europe* (2nd ed., p. 239). Shell Internationale Petroleum Mij. B.V. and Geologicasl Society of London.